Efficient organic room-temperature phosphorescence in both solution and solid states

Chensen Li[1,2,9], Zhenchen Lou[3,9], Minghui Wu[4,9], Xinmeng Chen[1], Haozhe Tan[2], Zonghang Liu[2], Feng Gao[2], Zijie Qiu[2], Zheng Zhao*[2], Lianrui Hu*[3], Guohua Xie*[5], Maoqiu Li[6], Yumeng Guo[6], Zhongjie Ren*[6], Song Zhang[7], Yuchao Liu[8], Shouke Yan[6,8], Ryan T. K. Kwok[1], Jacky W. Y. Lam[1], Ben Zhong Tang*[1,2]

1. *Department of Chemistry and Hong Kong Branch of Chinese National Engineering Research Center for Tissue Restoration and Reconstruction, The Hong Kong University of Science and Technology, Kowloon, Hong Kong, China.*
2. *School of Science and Engineering, Shenzhen Institute of Aggregate Science and Technology, The Chinese University of Hong Kong, Shenzhen (CUHK-Shenzhen), Guangdong 518172, China.*
3. *Shanghai Key Laboratory of Green Chemistry and Chemical Processes, Shanghai Frontiers Science Center of Molecule Intelligent Syntheses, School of Chemistry and Molecular Engineering, East China Normal University, 3663 N. Zhongshan Road, Shanghai 200062, China.*
4. *Department of Chemistry, Southern University of Science and Technology, Shenzhen 518055, China.*
5. *The Institute of Flexible Electronics (Future Technologies), Xiamen University, Xiamen 361005, China.*
6. *State Key Laboratory of Chemical Resource Engineering, College of Materials Science and Engineering, Beijing University of Chemical Technology, Beijing 100029, China.*
7. *State Key Laboratory of Magnetic Resonance and Atomic and Molecular Physics, Wuhan Institute of Physics and Mathematics, Chinese Academy of Sciences, Wuhan 430071, China.*
8. *Key Laboratory of Rubber-Plastics, Ministry of Education, Qingdao University of Science & Technology, Qingdao, 266042, China.*

Synthesis

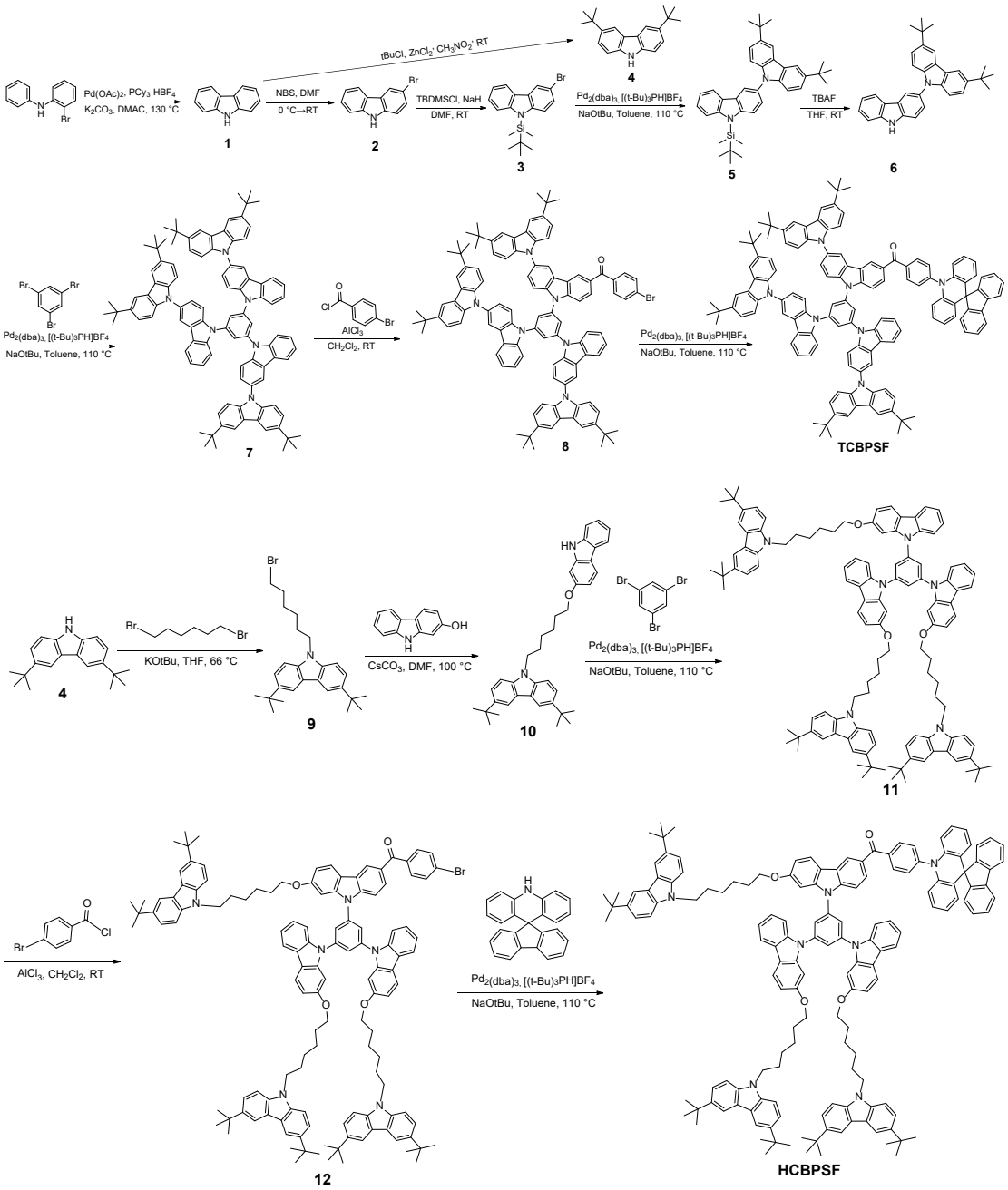

Scheme S1. The synthesis routes of TCBPSF and HCBPSF.

9*H*-carbazole (1)

9*H*-carbazole was prepared according to the previous reference.[1] N-(2bromophenyl)aniline (2.5 g, 10 mmol), K_2CO_3 (2.8 g, 20 mmol), $Pd(OAc)_2$ (0.23 g, 1.0 mmol) and PCy_3-HBF_4 (0.74 g, 2.0 mmol) were placed in a 100 mL round bottom flask. The flask was purged with argon for 3 times, and 50 mL (0.2 M) of degassed *N,N*-dimethylacetamide (DMAc) was added. The reaction was heated and stirred to 130 ºC

for 12 hours. After the reaction was completed, the heat source was removed, and the reaction mixture was cooled to room temperature. The resulted mixture was then extracted with DCM for 3 times, and the combined organic phase was dried over anhydrous Na_2SO_4, filtered, and then evaporated under reduced pressure. The crude material was purified by column chromatography for 3 times with eluents at the ratio of DCM/hexane = 1/3 v/v to yield as white powders (1.4 g, 84% yield). ^{1}H NMR (500 MHz, DMSO-d6): 11.26 (s, 1H), 8.11 (d, 2H), 7.50 (d, 2H), 7.39 (t, 2H), 7.16 (t, 2H).

3-bromo-9H-carbazole (2)

3-bromo-9*H*-carbazole was prepared according to the previous reference.[2] Carbazole (1.002 g, 5.997 mmol) was added into DMF solution (50 mL). Then the mixture of N-bromosuccinimide (NBS) (1.068 g, 6.00 mmol) and DMF (20 mL) was added dropwise into reaction flask in ice-water bath. After filtration and washed by water, and then purified by silica gel column chromatography using dichloromethane/hexane (1/10 v/v) to give the pure product white powder (1.254 g, 85.0%). ^{1}H NMR (500 MHz, DMSO) δ 11.44 (s, 1H), 8.37 (s, 1H), 8.17 (d, J = 7.8 Hz, 1H), 7.50 (d, J = 7.5 Hz, 2H), 7.46 (d, J = 8.6 Hz, 1H), 7.45 – 7.40 (m, 1H), 7.19 (t, J = 7.19 Hz, 1H).

3-bromo-9-(*tert*-butyldimethylsilyl)-9*H*-carbazole (3)

3-bromo-9*H*-carbazole (2.46 g, 10.0 mmol) was dissolved in dry DMF and then NaH (0.36 g, 15.0 mmol) was added in batches at room temperature. Next, a solution of *tert*-butyldimethylchlorosilane (2.27 g, 15.0 mmol) in dry DMF (30 mL) was added dropwise. After stirring for 8 h, the mixture was poured into water and filtered to give the crude product, which was then purified by silica gel column chromatography using dichloromethane/hexane (1/10 v/v) to give the pure product as a white solid (3.6 g, 82% yield). ^{1}H NMR (500 MHz, $CDCl_3$) δ 8.18 (d, J = 1.8 Hz, 1H), 8.03 (d, J = 7.8 Hz, 1H), 7.62 (d, J = 8.4 Hz, 1H), 7.47 (dt, J = 8.8, 5.4 Hz, 2H), 7.43 – 7.38 (m, 1H), 7.26 (d, J = 7.1 Hz, 1H), 1.05 (s, 9H), 0.77 (s, 6H).

3,6-di-tert-butyl-9H-carbazole (4)

9-*H*-carbazole (3.3 g, 20 mmol), 100 ml of nitromethane, and $ZnCl_2$ (8.1 g, 60 mmol) were added to a three-neck flask under a nitrogen atmosphere. 2-Chloro-2-methylpropane (6.5 ml, 60 mmol) was added dropwise under stirring. The mixture was stirred at room temperature for 8 h and then hydrolyzed with 100 ml of water. The product was extracted with CH_2Cl_2. The organic layer was washed with H_2O, dried with $MgSO_4$, and evaporated under vacuum to yield 5.2 g (94 %) of white solid. ^{1}H NMR (400 MHz, $CDCl_3$) δ 8.10 (s, 2H), 7.88 (s, 1H), 7.49 (dd, *J*= 7.6, 0.9 Hz, 2H), 7.36 (d, *J* = 8.5 Hz, 2H), 1.48 (s, 18H).

3',6'-di-*tert*-butyl-9-(*tert*-butyldimethylsilyl)-9*H*-3,9'-bicarbazole (5)

A mixture of compound 3-bromo-9-(*tert*-butyldimethylsilyl)-9*H*-carbazole (**3**) (361 mg, 1 mmol), 3,6-di-*tert*-butyl-9*H*-carbazole (280 mg, 1 mmol), tris(dibenzylideneacetone)dipalladium ($Pd_2(dba)_3$) (38 mg, 0.037 mmol), $(t\text{-}Bu)_3PHBF_4$ (21 mg, 0.073 mol) and sodium tert-butoxide (NaO^tBu) (210 mg, 2.19 mmol) in toluene (20 mL) was stirred at 110 °C under argon for 24 h. After cooling to room temperature, the mixture was washed with brine and the organic phase was separated and dried with anhydrous sodium sulfate. After filtration and removal of the solvent, the product mixture was applied to a silica gel column using hexane/dichloromethane (8/1 v/v) as eluent to give the crude product as white power. The powder was further crystallized from a mixture of hexane and CH_2Cl_2 to afford the pure product (497 mg, 89% yield) as a white powder. ^{1}H NMR (400 MHz, $CDCl_3$) δ 8.36 (dd, *J* = 5.7, 1.8 Hz, 3H), 8.15 (d, *J* = 7.3 Hz, 1H), 7.90 (d, *J* = 8.8 Hz, 1H), 7.80 (d, *J* = 8.5 Hz, 1H), 7.62 (m, *J* = 15.3, 8.7, 2.0 Hz, 3H), 7.54 (dt, *J* = 17.1, 4.9 Hz, 3H), 7.37 (t, *J* = 7.3 Hz, 1H), 1.64 (s, 18H), 1.25 (s, 9H), 0.95 (s, 6H). ^{13}C NMR (101 MHz, $CDCl_3$) δ 145.27, 143.47, 141.89, 139.76, 129.62, 126.92, 125.49, 125.40, 124.00, 123.00, 122.58, 119.58, 119.45, 118.01, 115.68, 114.36, 113.86, 108.82, 34.26, 31.63, 26.13, 20.15. MALDI-MS$^+$: m/z: calculated for $C_{38}H_{46}N_2Si$: 558.3430 [M^+]; found: 559.3494 [$M+H]^+$.

3',6'-di-*tert*-butyl-9*H*-3,9'-bicarbazole (6)

3',6'-di-*tert*-butyl-9-(*tert*-butyldimethylsilyl)-9*H*-3,9'-bicarbazole (**5**) (5.59 g, 10 mmol) was dissolved in dry THF (50 mL), and then tetrabutylammonium fluoride (2.62 g, 10 mmol) was added. The mixture was stirred at 25 °C for 4 h, followed by pouring into water and filtration. The solid residue was collected and applied onto a silica gel column eluted with dichloromethane/hexane (1/3 v/v) to give the product as a white solid (4.05 g, 91% yield). ^{1}H NMR (400 MHz, $CDCl_3$) δ 8.22 (d, *J* = 8.9 Hz, 4H), 8.05 (d, *J* = 7.8 Hz, 1H), 7.56 (dt, *J* = 8.5, 5.0 Hz, 2H), 7.51 – 7.45 (m, 4H), 7.33 (d, *J* = 8.6 Hz, 2H), 7.27 (s, 1H), 1.50 (s, 18H). ^{13}C NMR (101 MHz, $CDCl_3$) δ 141.79, 139.68, 139.54, 137.75, 129.32, 125.86, 124.69, 123.68, 122.89, 122.45, 122.37, 119.95, 119.22, 118.65, 115.57, 110.88, 110.27, 108.57, 34.13, 31.46, 25.04. MALDI-MS^{+}: m/z: calculated for $C_{32}H_{32}N_2$: 444.6220 [M^{+}]; found: 445.6241 [M+H]$^{+}$.

1,3,5-tris(3',6'-di-*tert*-butyl-9*H*-[3,9'-bicarbazol]-9-yl)benzene (7)

A mixture of compound 3',6'-di-*tert*-butyl-9*H*-3,9'-bicarbazole (**6**) (445 g, 1 mmol), 1,3,5-tribromobenzene (105 mg, 0.33 mmol), tris(dibenzylideneacetone)dipalladium ($Pd_2(dba)_3$) (38 mg, 0.037 mmol), $(t\text{-}Bu)_3PHBF_4$ (21 mg, 0.073 mol) and sodium tert-butoxide (NaO^tBu) (210 mg, 2.19 mmol) in toluene (20 mL) was stirred at 110 °C under argon for 24 h. After cooling to room temperature, the mixture was washed with brine and the organic phase was separated and dried with anhydrous sodium sulfate. After filtration and removal of the solvent, the product mixture was applied to a silica gel column using hexane/dichloromethane (3/1 v/v) as eluent to give the crude product as white power. The powder was further crystallized from a mixture of hexane and CH_2Cl_2 to afford the pure product (379 mg, 81% yield) as a white powder. ^{1}H NMR (400 MHz, $CDCl_3$) δ 8.36 (s, 1H), 8.20 (dd, *J* = 13.9, 6.3 Hz, 4H), 7.93 (d, *J* = 8.6 Hz, 1H), 7.82 (d, *J* = 8.3 Hz, 1H), 7.69 (d, *J* = 8.6 Hz, 1H), 7.60 (t, *J* = 7.8 Hz, 1H), 7.49 (d, *J* = 8.7 Hz, 2H), 7.43 (t, *J* = 7.5 Hz, 1H), 7.38 (d, *J* = 8.6 Hz, 2H), 1.50 (s, 18H). ^{13}C NMR (101 MHz, $CDCl_3$) δ 142.08, 140.41, 139.54, 138.58, 130.87, 126.60, 125.25, 124.46, 123.23, 123.04, 122.61, 120.76, 120.43, 118.92, 115.74, 110.16, 109.43, 108.52, 34.20, 31.51, 31.05, 29.17, 22.12, 13.60. MALDI-MS^{+}: m/z: calculated for $C_{102}H_{96}N_6$: 1404.7696 [M^{+}]; found: 1405.7775 [M+H]$^{+}$.

(9-(3,5-bis(3',6'-di-*tert*-butyl-9*H*-[3,9'-bicarbazol]-9-yl)phenyl)-3',6'-di-*tert*-butyl-9*H*-[3,9'-bicarbazol]-6-yl)(4-bromophenyl)methanone (8)

Aluminum trichloride (112 mg, 0.84 mmol) was added to a stirred solution of 1,3,5-tris(3',6'-di-*tert*-butyl-9*H*-[3,9'-bicarbazol]-9-yl)benzene (7) (1.587 g, 1 mmol) and 4-bromobenzoyl chloride (200 mg, 0.91 mmol) in dehydrated dichloromethane (50 mL) in ice bath for 15 minutes. Then the reaction mixture was warmed to room temperature and stirred for 3 h. The reaction was quenched with ice water and hydrochloric acid (15 mL, 2/1 v/v), and extracted with dichloromethane several times. The combined organic layers were washed twice with water, and then dried over anhydrous $MgSO_4$. After filtration and solvent evaporation under reduced pressure, the residue was purified by column chromatography using dichloromethane/hexane (1/1 v/v) to afford a green solid in 45% yield. ^{1}H NMR (400 MHz, $CDCl_3$) δ 8.36 (d, *J* = 8.6 Hz, 3H), 8.24 – 8.17 (m, 8H), 8.12 (s, 2H), 7.95 (dd, *J* = 16.2, 8.2 Hz, 3H), 7.80 (t, *J* = 9.8 Hz, 3H), 7.70 (s, 3H), 7.64 – 7.56 (m, 4H), 7.48 (d, *J* = 8.0 Hz, 6H), 7.45 – 7.34 (m, 8H), 7.18 (d, *J* = 8.7 Hz, 1H), 7.10 (d, *J* = 8.1 Hz, 1H), 7.01 (s, 3H), 1.49 (s, 54H). ^{13}C NMR (101 MHz, $CDCl_3$) δ 196.02, 143.66, 142.87, 141.10, 130.87, 130.55, 127.24, 124.84, 124.45, 123.88, 123.64, 123.47, 122.76, 122.34, 121.28, 121.07, 119.57, 117.68, 116.27, 109.59, 106.03, 35.22, 34.92, 34.86, 34.81, 32.10, 32.06, 32.00, 31.94, 31.84, 29.77. MALDI-MS$^+$: m/z: calculated for $C_{109}H_{99}BrN_6O$ $[M]^+$: 1586.7064; found: 1587.7070 $[M+H]^+$.

(4-(10*H*-spiro[acridine-9,9'-fluoren]-10-yl)phenyl)(9-(3,5-bis(3',6'-di-*tert*-butyl-9*H*-[3,9'-bicarbazol]-9-yl)phenyl)-3',6'-di-*tert*-butyl-9*H*-[3,9'-bicarbazol]-6-yl)methanone (TCBPSF)

A mixture of compound (9-(3,5-bis(3',6'-di-*tert*-butyl-9*H*-[3,9'-bicarbazol]-9-yl)phenyl)-3',6'-di-*tert*-butyl-9*H*-[3,9'-bicarbazol]-6-yl)(4-bromophenyl)methanone (**8**) (1.587 g, 1 mmol), 10H-spiro[acridine-9,9'-fluorene] (332 mg, 1 mmol), tris(dibenzylideneacetone)dipalladium ($Pd_2(dba)_3$) (38 mg, 0.037 mmol), (t-Bu)$_3$PHBF$_4$ (21 mg, 0.073 mol) and sodium tert-butoxide (NaO^tBu) (210 mg, 2.19 mmol) in toluene (20 mL) was stirred at 110 °C under argon for 24 h. After cooling to

room temperature, the mixture was washed with brine and the organic phase was separated and dried with anhydrous sodium sulfate. After filtration and removal of the solvent, the product mixture was applied to a silica gel column using hexane/dichloromethane (1/1 v/v) as eluent to give the crude product as white power. The powder was further crystallized from a mixture of hexane and CH_2Cl_2 to afford the pure product (1.43 g, 78% yield) as a green powder. ^{1}H NMR (400 MHz, $CDCl_3$) δ 8.55 (d, *J* = 1.8 Hz, 1H), 8.43 (dd, *J* = 5.9, 1.8 Hz, 2H), 8.39 (d, *J* = 1.5 Hz, 1H), 8.32 – 8.28 (m, 6H), 8.20 (ddd, *J* = 14.0, 12.2, 4.4 Hz, 6H), 7.93 (d, *J* = 8.1 Hz, 2H), 7.88 – 7.83 (m, 2H), 7.82 (d, *J* = 1.9 Hz, 2H), 7.78 (d, *J* = 7.0 Hz, 3H), 7.64 (d, *J* = 8.3 Hz, 4H), 7.60 – 7.53 (m, 6H), 7.50 – 7.42 (m, 10H), 7.36 – 7.29 (m, 6H), 7.14 (t, *J* = 9.3 Hz, 2H), 6.83 (t, *J* = 7.0 Hz, 2H), 6.55 (dd, *J* = 13.9, 7.1 Hz, 2H), 6.39 (dd, *J* = 21.2, 7.6 Hz, 4H), 1.37 (s, 54H). ^{13}C NMR (101 MHz, $CDCl_3$) δ 195.83, 155.37, 144.53, 143.29, 142.58, 142.05, 140.57, 140.39, 140.14, 139.56, 138.58, 138.26, 137.21, 136.99, 132.19, 131.15, 130.89, 130.18, 127.75, 127.30, 127.06, 126.62, 126.30, 125.24, 125.02, 124.71, 124.50, 124.18, 123.07, 122.63, 122.49, 122.19, 120.77, 120.41, 119.30, 119.07, 117.03, 115.71, 113.76, 110.14, 109.37, 109.12, 108.57, 105.43, 56.10, 52.86, 34.42, 34.29, 34.22, 31.55, 31.47, 31.31, 31.26, 31.08, 29.20, 22.15, 13.63. MALDI-MS$^+$: m/z: calculated for $C_{134}H_{115}N_7O$: 1837.9163 $[M]^+$; found: 1838.9227$[M+H]^+$.

9-(6-bromohexyl)-3,6-di-*tert*-butyl-9*H*-carbazole (9)

To a solution of compound 3,6-di-*tert*-butyl-9*H*-carbazole (**4**) (1.4 g, 5 mmol) in dry THF (10 mL) was added KO^{t}Bu (0.706 g, 6.3 mmol) in several portions. The resulting solution was stirred for 10 min at room temperature, and then added dropwise to a refluxing solution of 1,6-dibromohexane (4.5 mL, 29.2 mmol) in THF (10 mL). After refluxing for 24 h, the reaction mixture was cooled to room temperature and quenched by adding several drops of water to destroy the excessive KO^{t}Bu. The THF solvent and excess 1,6-dibromohexane were removed by rotatory evaporation and vacuum distillation, respectively. The residual product was dissolved in CH_2Cl_2, washed with water for three times, the organic layer was dried over anhydrous Na_2SO_4, filtered and concentrated for flash column chromatography on silica using CH_2Cl_2/petroleum ether

(1/10 v/v), affording product as a white solid (1.76 g 80% yield). ^{1}H NMR (400 MHz, $CDCl_3$) δ 8.15 (d, *J* = 1.7 Hz, 1H), 7.55 (dd, *J* = 8.6, 1.9 Hz, 1H), 7.33 (d, *J* = 8.6 Hz, 1H), 4.28 (t, *J* = 7.1 Hz, 1H), 3.39 (t, *J* = 6.7 Hz, 1H), 1.95 – 1.77 (m, 2H), 1.51 (s, 9H), 1.49 – 1.39 (m, 2H). ^{13}C NMR (101 MHz, $CDCl_3$) δ 140.90, 138.34, 122.67, 122.07, 115.70, 107.37, 42.34, 34.07, 33.23, 32.00, 31.50, 28.40, 27.37, 25.91. MALDI-MS$^+$: m/z: calculated for $C_{26}H_{36}BrN$: 441.2031 $[M]^+$; found: 441.2026 $[M]^+$.

9-(6-((9*H*-carbazol-2-yl)oxy)hexyl)-3,6-di-*tert*-butyl-9*H*-carbazole (10)

A mixture of 9-(6-bromohexyl)-3,6-di-*tert*-butyl-9*H*-carbazole (9) (441 mg, 1.0 mmol), 9H-carbazol-2-ol (183 mg, 1.0 mmol) and Cs_2CO_3 (391 mg, 1.2 mmol) in N,N-dimethylformamide (10 mL)solution was heated at 100 °C under nitrogen for 24 h. After cooling, the mixture was poured into water (200 mL). The crude product was filtered and purified by silica gel column chromatography, eluent CH_2Cl_2/petroleum ether (1/2 v/v). The product was recrystallized from ethyl acetate to give product as a white powder (462 mg, 85%). ^{1}H NMR (400 MHz, $CDCl_3$) δ 8.31 (d, *J* = 7.7 Hz, 1H), 8.11 (d, *J* = 1.6 Hz, 2H), 8.06 (s, 1H), 7.50 (dd, *J* = 8.6, 1.9 Hz, 2H), 7.43 – 7.35 (m, 2H), 7.34 – 7.29 (m, 3H), 7.23 (m, *J* = 8.1, 6.4, 1.8 Hz, 1H), 7.03 (d, *J* = 8.0 Hz, 1H), 6.65 (d, *J* = 7.9 Hz, 1H), 4.34 – 4.14 (m, 4H), 2.03 – 1.88 (m, 4H), 1.74 – 1.62 (m, 2H), 1.54 (dd, *J* = 15.2, 7.0 Hz, 2H), 1.47 (s, 18H). ^{13}C NMR (101 MHz, $CDCl_3$) δ 140.80, 138.34, 126.05, 124.24, 122.63, 122.35, 122.01, 119.00, 115.63, 109.28, 107.38, 100.41, 67.07, 42.40, 34.03, 31.45, 28.71, 26.50, 25.55. MALDI-MS$^+$: m/z: calculated for $C_{38}H_{44}N_2O$: 544.3454 $[M]^+$; found: 544.3412 $[M]^+$.

1,3,5-tris(2-((6-(3,6-di-*tert*-butyl-9H-carbazol-9-yl)hexyl)oxy)-9*H*-carbazol-9-yl)benzene (11)

A mixture of compound 9-(6-((9*H*-carbazol-2-yl)oxy)hexyl)-3,6-di-*tert*-butyl-9*H*-carbazole (10) (554 mg, 1 mmol), 1,3,5-tribromobenzene (105 mg, 0.33 mmol), tris(dibenzylideneacetone)dipalladium ($Pd_2(dba)_3$) (38 mg, 0.037 mmol), (t-Bu)$_3$PHBF$_4$ (21 mg, 0.073 mol) and sodium tert-butoxide (NaO^tBu) (210 mg, 2.19 mmol) in toluene (20 mL) was stirred at 110 °C under argon for 24 h. After cooling to

room temperature, the mixture was washed with brine and the organic phase was separated and dried with anhydrous sodium sulfate. After filtration and removal of the solvent, the product mixture was applied to a silica gel column using hexane/dichloromethane (3/1 v/v) as eluent to give the crude product as white power. The powder was further crystallized from a mixture of hexane and CH_2Cl_2 to afford the pure product (382 mg, 82% yield) as a white powder. ^{1}H NMR (400 MHz, $CDCl_3$) δ 8.53 (d, *J* = 7.7 Hz, 1H), 8.24 (d, *J* = 1.6 Hz, 2H), 8.06 (s, 1H), 7.75 (d, *J* = 8.2 Hz, 1H), 7.60 (dd, *J* = 8.6, 1.9 Hz, 2H), 7.53 (dd, *J* = 11.4, 4.1 Hz, 1H), 7.48 – 7.35 (m, 5H), 6.82 (d, *J* = 8.0 Hz, 1H), 4.37 (t, *J* = 7.0 Hz, 2H), 4.30 (t, *J* = 6.2 Hz, 2H), 2.04 (dt, *J* = 14.6, 9.4 Hz, 4H), 1.77 (dd, *J* = 14.7, 7.8 Hz, 2H), 1.65 (s, 2H), 1.58 (s, 18H). ^{13}C NMR (101 MHz, $CDCl_3$) δ 155.91, 141.85, 141.54, 140.87, 139.69, 139.08, 127.29, 125.49, 123.80, 123.51, 123.43, 123.38, 122.78, 121.02, 116.37, 113.14, 109.19, 108.13, 102.52, 68.01, 43.11, 34.78, 32.22, 31.74, 29.86, 29.42, 29.31, 27.23, 26.29, 22.81, 14.31. MALDI-MS$^+$: m/z: calculated for $C_{120}H_{132}N_6O_3$: 1705.0361 $[M]^+$; found: 1706.0444 $[M+H]^+$.

(9-(3,5-bis(2-((6-(3,6-di-*tert*-butyl-9*H*-carbazol-9-yl)hexyl)oxy)-9*H*-carbazol-9-yl)phenyl)-7-((6-(3,6-di-*tert*-butyl-9*H*-carbazol-9-yl)hexyl)oxy)-9*H*-carbazol-3-yl)(4-bromophenyl)methanone (12)

Aluminum trichloride (112 mg, 0.84 mmol) was added to a stirred solution of 1,3,5-tris(2-((6-(3,6-di-*tert*-butyl-9H-carbazol-9-yl)hexyl)oxy)-9*H*-carbazol-9-yl)benzene (9) (1.71 g, 1 mmol) and 4-bromobenzoyl chloride (200 mg, 0.91 mmol) in dehydrated dichloromethane (50 mL) in ice bath for 15 minutes. Then the reaction mixture was warmed to room temperature and stirred for 3 h. The reaction was quenched with ice water and hydrochloric acid (15 mL, 2:1 v/v), and extracted with dichloromethane several times. The combined organic layers were washed twice with water, and then dried over anhydrous $MgSO_4$. After filtration and solvent evaporation under reduced pressure, the residue was purified by column chromatography on silica gel (dichloromethane/petroleum ether) to afford a green solid in 48% yield. ^{1}H NMR (400 MHz, $CDCl_3$) δ 8.92 – 8.70 (m, 4H), 8.57 – 8.46 (m, 5H), 8.45 – 8.38 (m, 1H), 8.30 (d, *J* = 28.7 Hz, 2H), 8.17 – 8.12 (m, 1H), 8.05 – 7.93 (m, 3H), 7.88 – 7.72 (m, 13H), 7.61

(dt, *J* = 16.6, 14.2 Hz, 14H), 7.45 (ddd, *J* = 26.9, 13.8, 5.6 Hz, 2H), 6.92 (s, 2H), 4.57 – 4.23 (m, 12H), 2.17 (m, 10H), 2.02 (m, 2H), 1.95 – 1.86 (m, 6H), 1.82 (s, 54H), 1.73 (m, 6H). ^{13}C NMR (101 MHz, $CDCl_3$) ^{13}C NMR (101 MHz, $CDCl_3$) δ 198.87, 195.05, 161.91, 155.53, 155.36, 145.07, 142.20, 141.47, 141.39, 141.35, 141.09, 140.86, 140.46, 140.09, 139.79, 139.34, 139.26, 138.72, 138.31, 137.35, 136.91, 136.65, 135.58, 131.81, 131.57, 131.10, 130.40, 128.28, 126.91, 125.87, 125.15, 125.05, 124.02, 123.25, 123.14, 123.00, 122.76, 122.47, 122.23, 122.08, 121.38, 120.67, 119.86, 119.16, 118.22, 116.08, 115.95, 115.72, 113.07, 112.89, 112.81, 112.63, 112.04, 111.75, 108.67, 108.25, 107.80, 102.12, 67.49, 60.00, 53.04, 42.57, 34.40, 34.35, 34.26, 31.84, 31.79, 31.76, 31.67, 31.63, 31.58, 31.38, 28.91, 28.79, 27.04, 26.78, 26.67, 26.13, 25.88, 25.58, 22.45, 22.27, 20.63, 13.94. MALDI-MS$^+$: m/z: calculated for $C_{127}H_{135}BrN_6O_4$: 1886.9728 $[M]^+$; found: 1887.9772 $[M+H]^+$.

(4-(10H-spiro[acridine-9,9'-fluoren]-10-yl)phenyl)(9-(3,5-bis(2-((6-(3,6-di-tert-butyl-9H-carbazol-9-yl)hexyl)oxy)-9H-carbazol-9-yl)phenyl)-7-((6-(3,6-di-tert-butyl-9H-carbazol-9-yl)hexyl)oxy)-9H-carbazol-3-yl)methanone (HCBPSF)

A mixture of compound (9-(3,5-bis(2-((6-(3,6-di-*tert*-butyl-9*H*-carbazol-9-yl)hexyl)oxy)-9*H*-carbazol-9-yl)phenyl)-7-((6-(3,6-di-*tert*-butyl-9*H*-carbazol-9-yl)hexyl)oxy)-9*H*-carbazol-3-yl)(4-bromophenyl)methanone (12) (1.89 g, 1 mmol), 10H-spiro[acridine-9,9'-fluorene] (332 mg, 1 mmol), tris(dibenzylideneacetone)dipalladium ($Pd_2(dba)_3$) (38 mg, 0.037 mmol), (t-Bu)$_3$PHBF$_4$ (21 mg, 0.073 mol) and sodium tert-butoxide (NaO^{t}Bu) (210 mg, 2.19 mmol) in toluene (20 mL) was stirred at 110 °C under argon for 24 h. After cooling to room temperature, the mixture was washed with brine and the organic phase was separated and dried with anhydrous sodium sulfate. After filtration and removal of the solvent, the product mixture was applied to a silica gel column using hexane/dichloromethane (1/1 v/v) as eluent to give the crude product as white power. The powder was further crystallized from a mixture of hexane and CH_2Cl_2 to afford the pure product (1.7 g, 79% yield) as a green powder. ^{1}H NMR (400 MHz, $CDCl_3$) δ 8.79 – 8.59 (m, 4H), 8.51 – 8.34 (m, 6H), 8.31 (d, *J* = 8.1 Hz, 1H), 8.22 (d, *J* = 10.3 Hz, 3H),

8.03 – 7.87 (m, 7H), 7.86 – 7.80 (m, 1H), 7.80 – 7.62 (m, 13H), 7.62 – 7.47 (m, 15H), 7.46 (d, J = 7.0 Hz, 2H), 7.41 – 7.29 (m, 1H), 7.21 (dd, J = 16.5, 8.3 Hz, 1H), 6.85 (ddd, J = 31.4, 18.3, 9.3 Hz, 5H), 6.75 – 6.63 (m, 3H), 4.44 (dd, J = 24.1, 17.5 Hz, 12H), 2.15 (s, 10H), 1.89 (dd, J = 31.5, 25.8 Hz, 8H), 1.74 (s, 54H), 1.63 (s, 6H). ^{13}C NMR (101 MHz, $CDCl_3$) δ 195.41, 155.96, 155.45, 145.46, 142.25, 141.33, 141.06, 140.56, 140.39, 139.77, 139.18, 138.84, 138.64, 138.24, 137.81, 135.63, 133.04, 131.36, 131.03, 128.04, 127.66, 127.32, 126.97, 126.84, 125.32, 125.12, 125.00, 124.80, 124.70, 123.21, 122.94, 122.67, 122.35, 122.14, 121.49, 120.74, 119.82, 119.60, 118.15, 116.05, 115.90, 114.09, 112.80, 112.70, 108.72, 108.20, 107.72, 102.07, 67.49, 56.39, 53.04, 42.57, 34.39, 34.31, 31.78, 31.73, 31.60, 31.27, 29.41, 28.91, 28.83, 26.96, 26.72, 26.27, 26.04, 25.82, 22.35, 13.88. MALDI-MS$^+$: m/z: calculated for $C_{152}H_{151}N_7O_4$: 2138.1828 $[M]^+$; found: 2139.0918 $[M+H]^+$.

Thermology properties

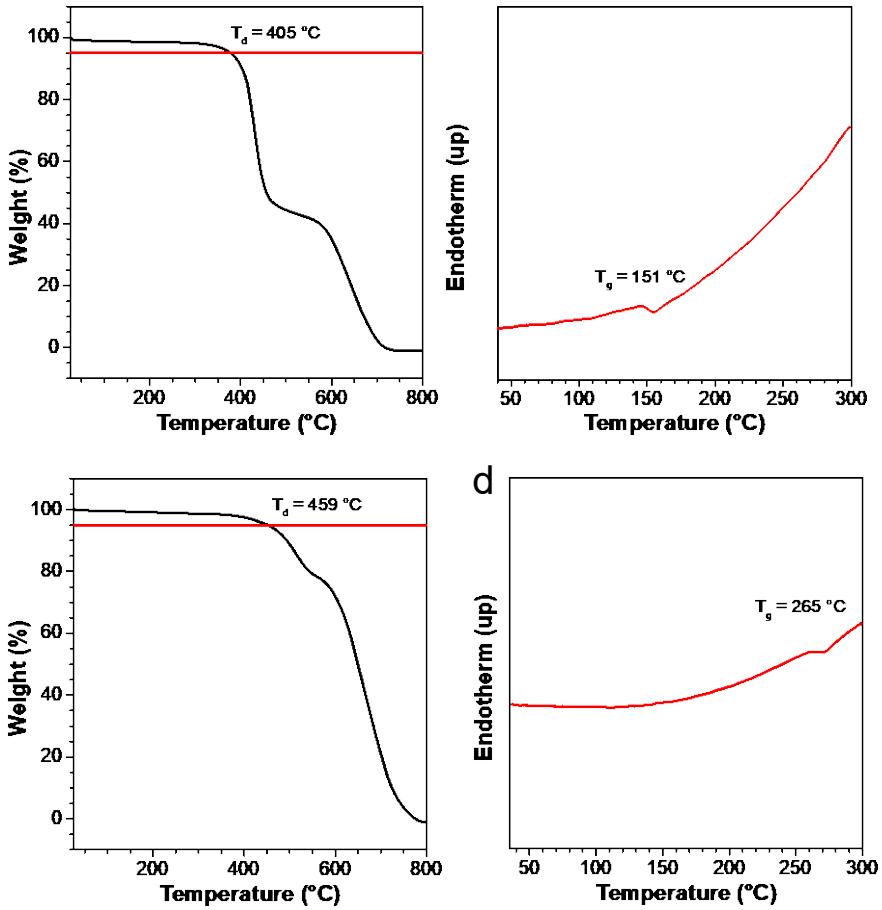

Fig. S1. TGA measurements of (**a**) TCBPSF and (**b**) HCBPSF and DSC traces of (**c**) TCBPSF and (**d**) HCBPSF recorded at a heating rate of 10 ºC/min under nitrogen atmosphere.

Electrochemical properties

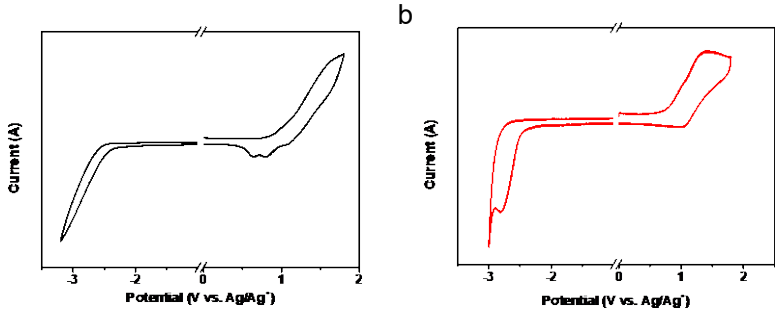

Fig. S2. Cyclic voltammetry curves of (**a**) TCBPSF and (**b**) HCBPSF.

Photophysical properties in solution

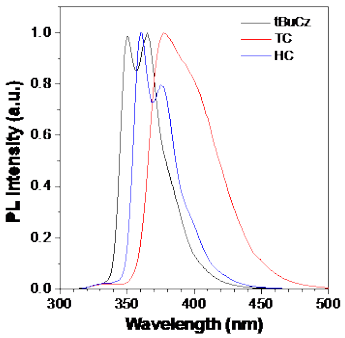

Fig. S3. The PL spectra of 3,6-di-tert-butylcarbazole (tBuCz), conjugated dendrons TC, and non-conjugated dendrons HC in dilute toluene.

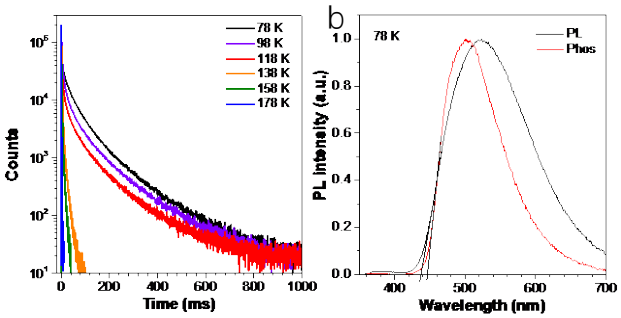

Fig. S4. (**a**) The temperature-dependent transient PL decay of TCBPSF from 78 to 178 K and (**b**) the PL and Phos spectra at 78 K in toluene.

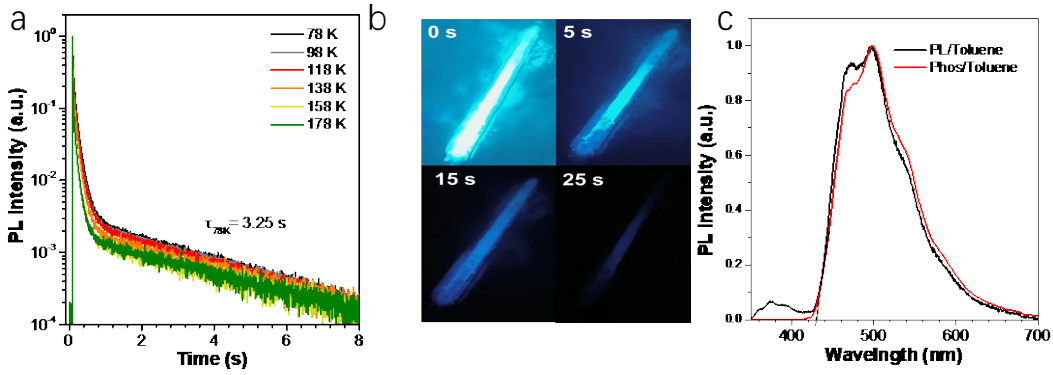

Fig. S5. (**a**) The temperature-dependent transient PL decay of HCBPSF from 78 to 178 K in toluene. (**b**) The photographs at different afterglow time of HCBPSF at 78 K in toluene. (**c**) the PL and Phos spectra at 78 K in toluene.

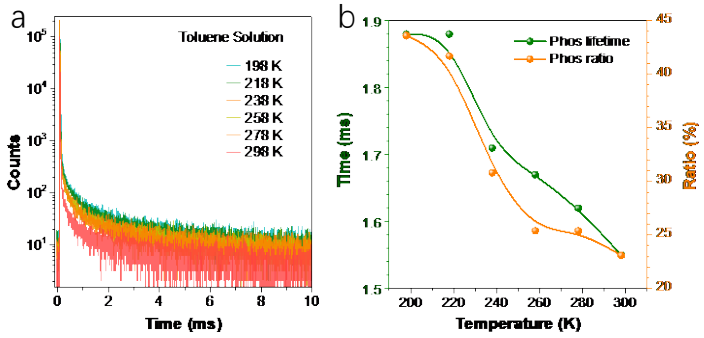

Fig. S6. (**a**) Temperature-dependent transient phosphorescence decay spectra of TCBPSF in toluene solution. (**b**) The plots of lifetimes and proportions of phosphorescence of TCBPSF at different temperature.

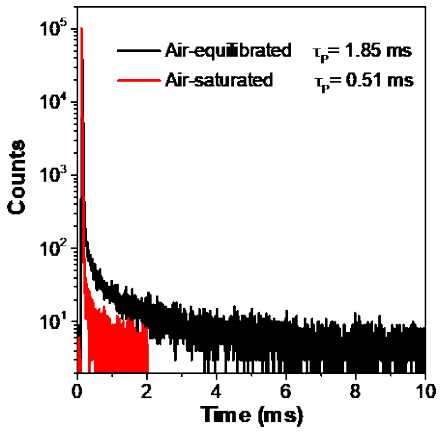

Fig. S7. The transient PL decay in air-equilibrated and air-saturated toluene.

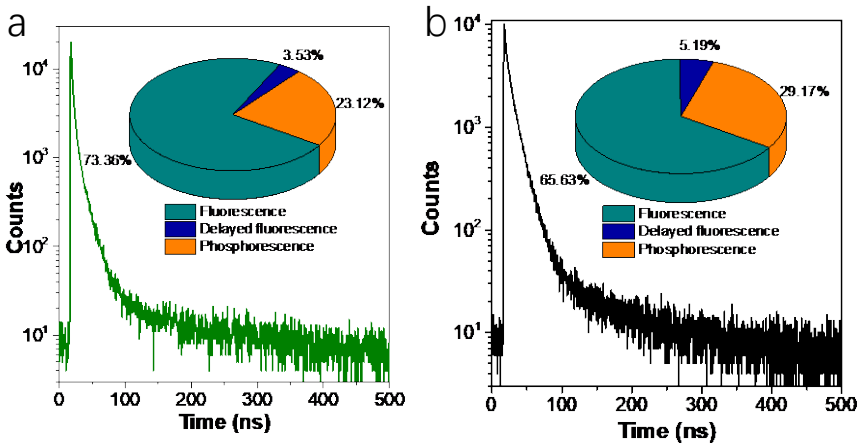

Fig. S8. The transient PL decay of TCBPSF (**a**) and HCBPSF (**b**) in sub-microsecond range and the proportions of fluorescence, delayed fluorescence, and phosphorescence spectra at 298 K. The phosphorescence proportions were calculated by the component of long-lived lifetime in millisecond range. The delayed fluorescence and fluorescence proportions were calculated by the component of long-lived and short-lived lifetime in microsecond range, respectively, as shown in **Table S1**.[6]

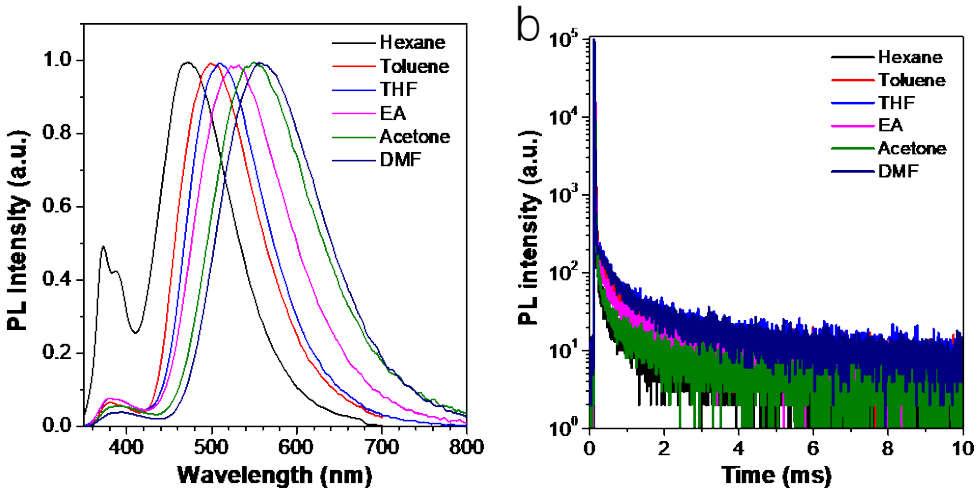

Fig. S9. The PL spectra of TCBPSF (**a**) and their transient PL decay (**b**) in different solvents.

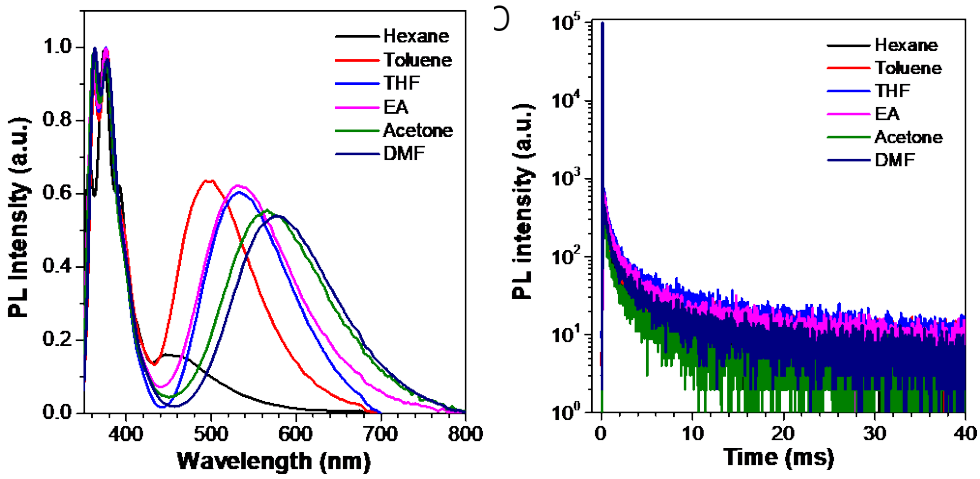

Fig. S10. The PL spectra of HCBPSF (**a**) and their transient PL decay (**b**) in different solvents.

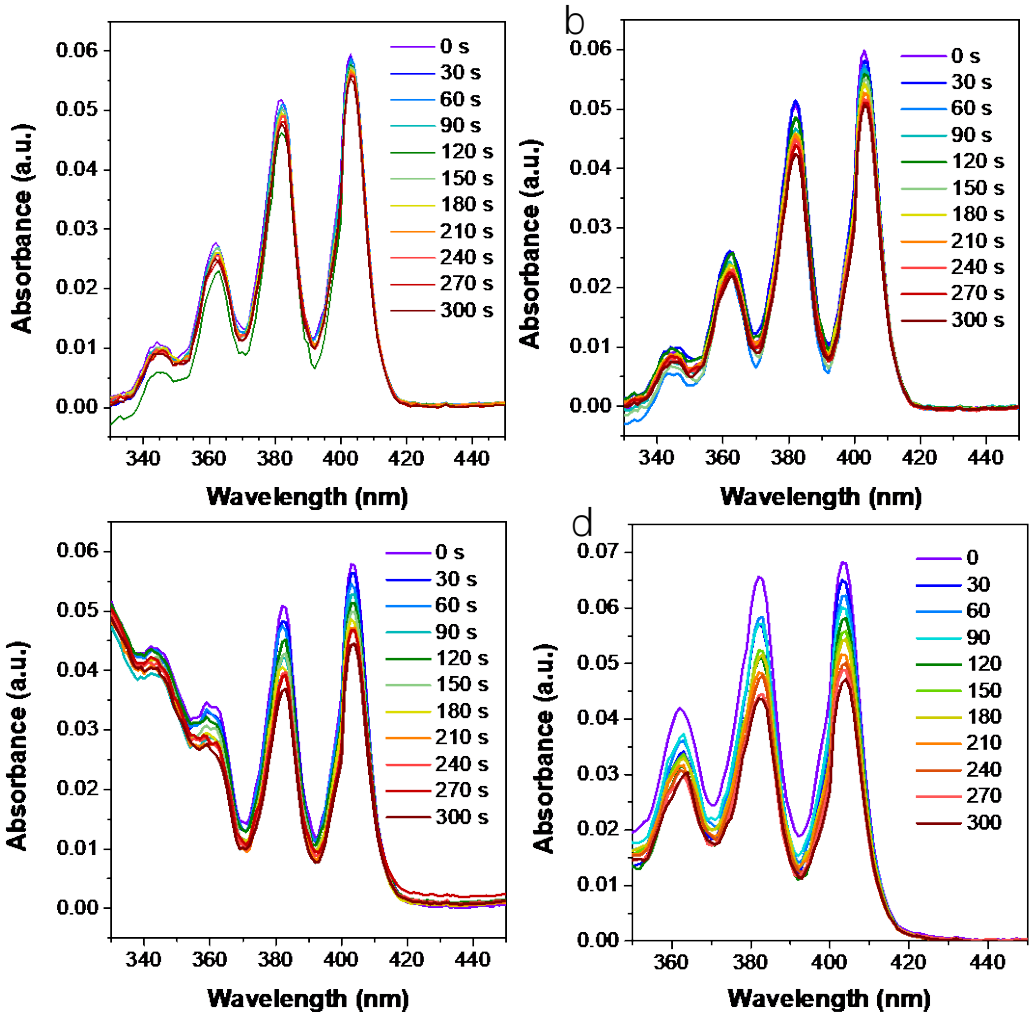

Fig. S11. The UV-vis spectra of ABDA in the presence of (**a**) blank control, HCBPSF (**b**), TCBPSF (**c**), and BPSF (**d**).

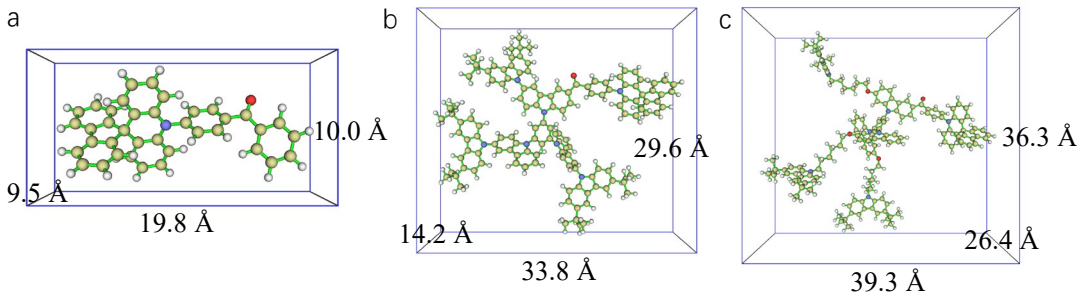

Fig. S12. The optimized geometrical and molecular volume of (**a**) BPSF, (**b**) TCBPSF, and (**c**) HCBPSF.

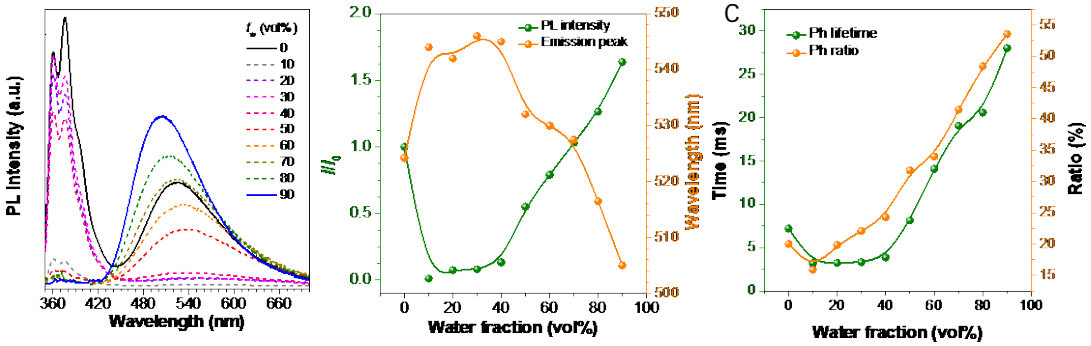

Fig. S13. (**a**) PL spectra of HCBPSF in water/THF mixtures with different water fractions (f_w). (**b**) Plots of relative PL intensity (I/I_0) and maximum emission wavelength with different f_w. I_0 = intensity at f_w = 10%. (**c**) The plot of the lifetimes and proportions of phosphorescence of HCBPSF in different ratios of mixtures solution.

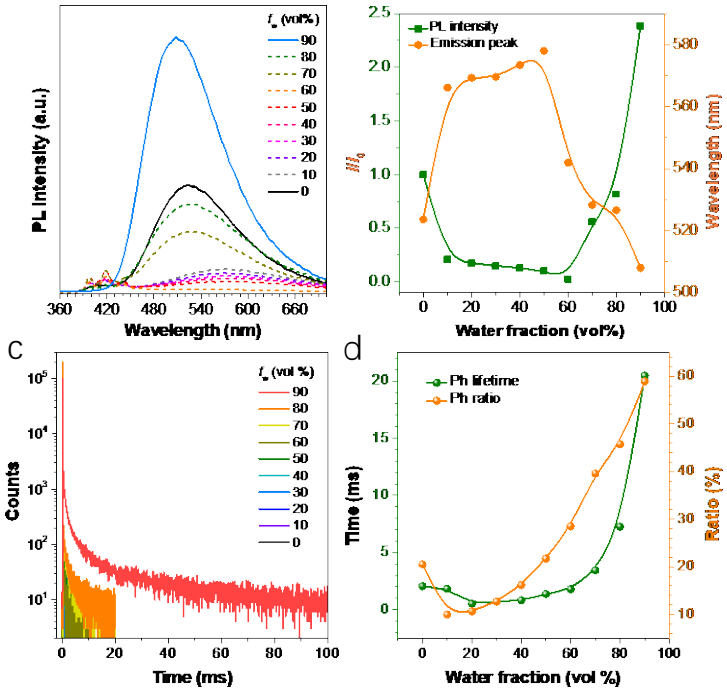

Fig. S14. (**a**) PL spectra of TCBPSF in water/THF mixtures with different water fractions (f_w). (**b**) Plots of relative PL intensity (I/I_0) and maximum emission wavelength with different f_w. I_0 = intensity at f_w = 10%. (**c**) Transient PL decay spectra of TCBPSF in water/THF mixtures with f_w. (**d**) The plot of the lifetimes and proportions of phosphorescence of TCBPSF in different ratios of mixtures solution.

Table S1. Summary of the detailed photophysical parameters of the investigated dendrimers in toluene and water/THF mixtures.

	TCBPSF (Toluene)	HCBPSF (Toluene)	10% water-TCBPSF	90% water - TCBPSF	10% water - HCBPSF	90% water-HCBPSF
τ_F (ns)	6.09	7.07	1.6	6.31	1.68	6.23
F [%]	73.4	65.7	87.5	26.4	79.7	45.7
τ_{DF} (ns)	46	99.5	7.21	180	78.9	388
DF [%]	3.5	5.06	3.4	36.5	6.6	19.4
τ_P (ms)	1.55	8.97	1.82	20.46	3.18	28.0
RTP [%]	23.1	29.2	9.1	37.1	13.7	34.9
φ_{PL} (%)	14	9	3	33	1	15
φ_F (%)	10.3	5.9	2.62	8.71	0.80	6.85
φ_{DF} (%)	0.49	0.46	0.10	12.05	0.066	2.91
φ_P (%)	3.2	2.6	0.27	12.24	0.14	5.24
k_F (10^6 s^{-1})	16.9	8.36	16.4	13.8	4.74	11.0
k_{RISC} (10^6 s^{-1})	2.35	0.643	3.79	1.31	0.11	0.26
k_P (s^{-1})	20.87	2.93	1.50	5.98	0.43	1.87
k_{nr} (10^2 s^{-1})	6.24	1.09	5.47	0.43	3.14	0.34
k_{ISC} (10^6 s^{-1})	6.11	4.36	2.34	38.5	1.21	13.1

Theoretical calculation

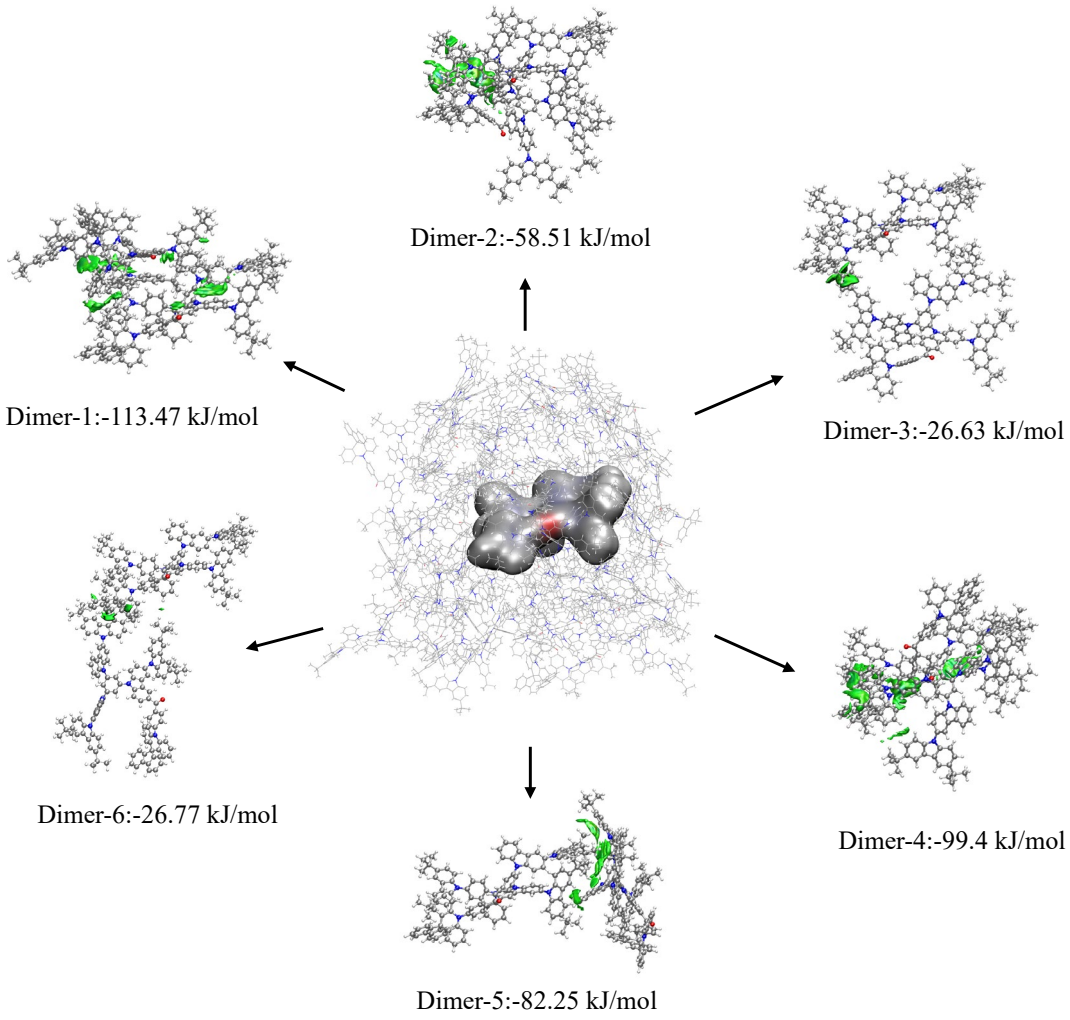

Fig. S15. The aggregate environment and the intermolecular interactions of TCBPSF was simulated using the ONIOM model with a combined quantum mechanics and molecular mechanics (QM/MM) approach. The central molecule acted as the high layer with QM at the B3LYP-D3/6-31G(d,p) level, while the surrounding molecules acted as the low layer using the universal force field (UFF).

Table S2. Summary of the detailed intermolecular interactions of TCBPSF in aggregate state.

Film	Dimer	Electrostatic (kJ/mol)	Repulsion (kJ/mol)	Dispersion (kJ/mol)	Total (kJ/mol)
SFAc-BP-CztCz	1	-1.24	49.95	-162.19	-113.47
	2	-2.13	53.79	-110.18	-58.51

	3	-0.68	12.12	-38.07	-26.63
	4	-4.92	39.71	-134.18	-99.4
	5	-1.16	43.07	-124.15	-82.25
	6	-0.01	3.79	-30.55	-26.77
	Average	-1.69	33.74	-99.89	-67.84

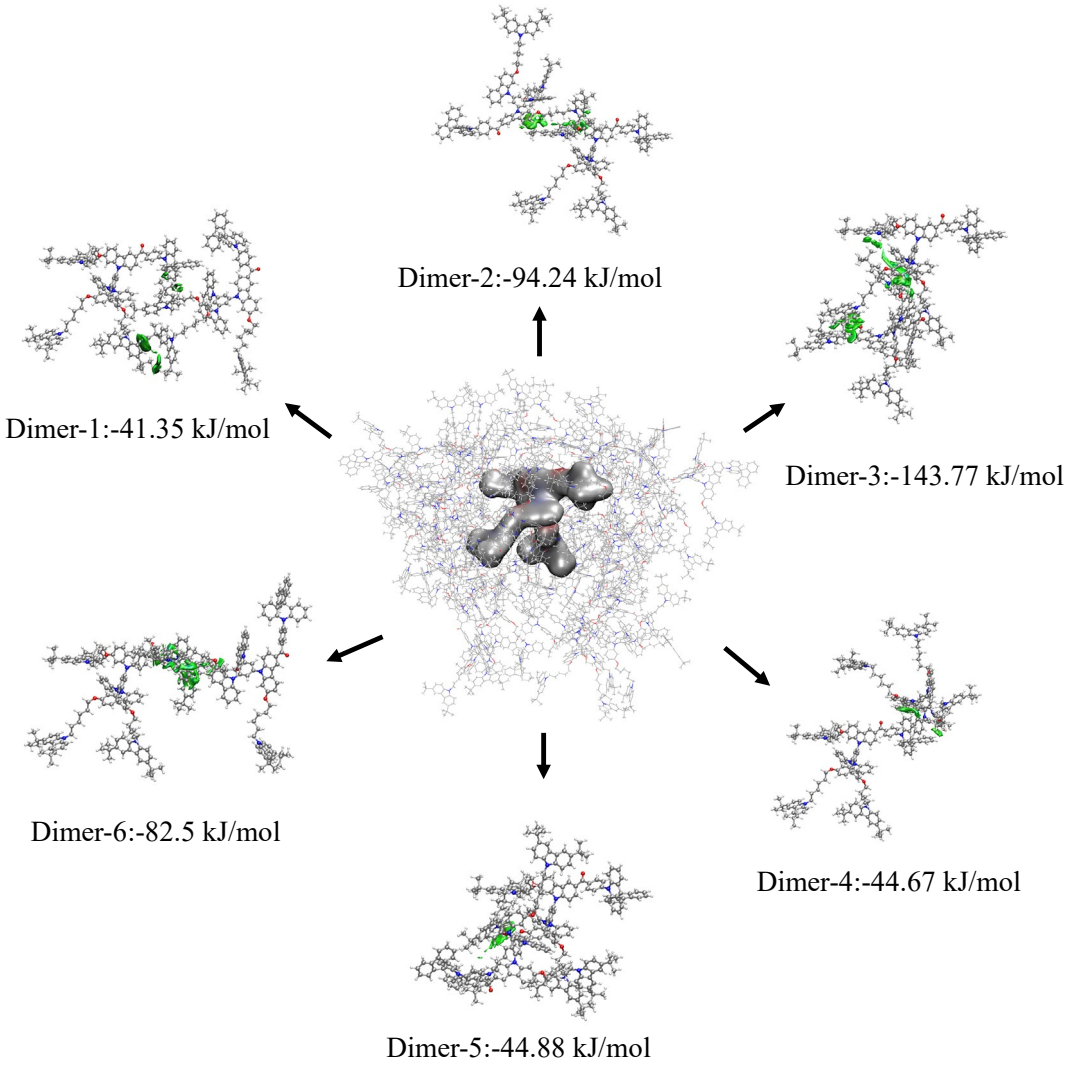

Fig. S16. The aggregate environment and the intermolecular interactions of HCBPSF was simulated using the ONIOM model with a combined quantum mechanics and molecular mechanics (QM/MM) approach. The central molecule acted as the high layer with QM at the B3LYP-D3/6-31G(d,p) level, while the surrounding molecules acted as the low layer using the universal force field (UFF).

Table S3. Summary of the detailed intermolecular interactions of HCBPSF in aggregate state.

Film	Dimer	Electrostatic (kJ/mol)	Repulsion (kJ/mol)	Dispersion (kJ/mol)	Total (kJ/mol)
SFAc-BP-HCz	1	-0.14	18.16	-59.37	-41.35
	2	-7.94	38.66	-124.96	-94.24
	3	-3.75	44.43	-184.45	-143.77
	4	-0.29	14.78	-59.16	-44.67
	5	-0.59	12.26	-56.55	-44.88
	6	-3.27	29.38	-108.62	-82.5
	Average	-2.66	26.28	-98.85	-75.24

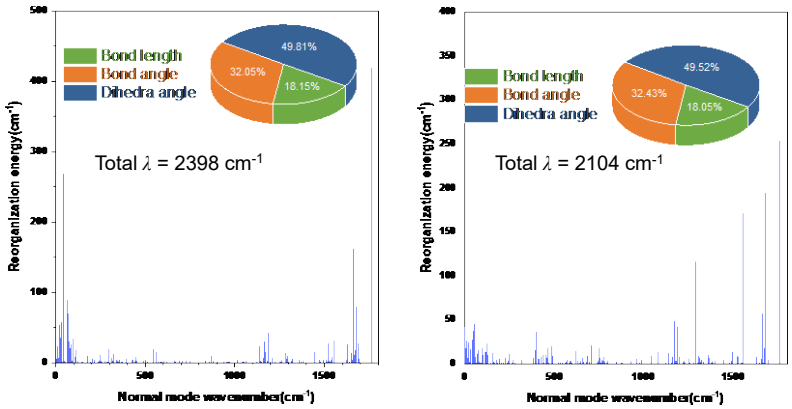

Fig. S17. Plots of reorganization energy (λ) vs normal mode wavenumber of TCBPSF (**a**) and HCBPSF (**b**). Inset: Proportions of bond length, bond angle, and dihedral angle contributed to total reorganization energy.

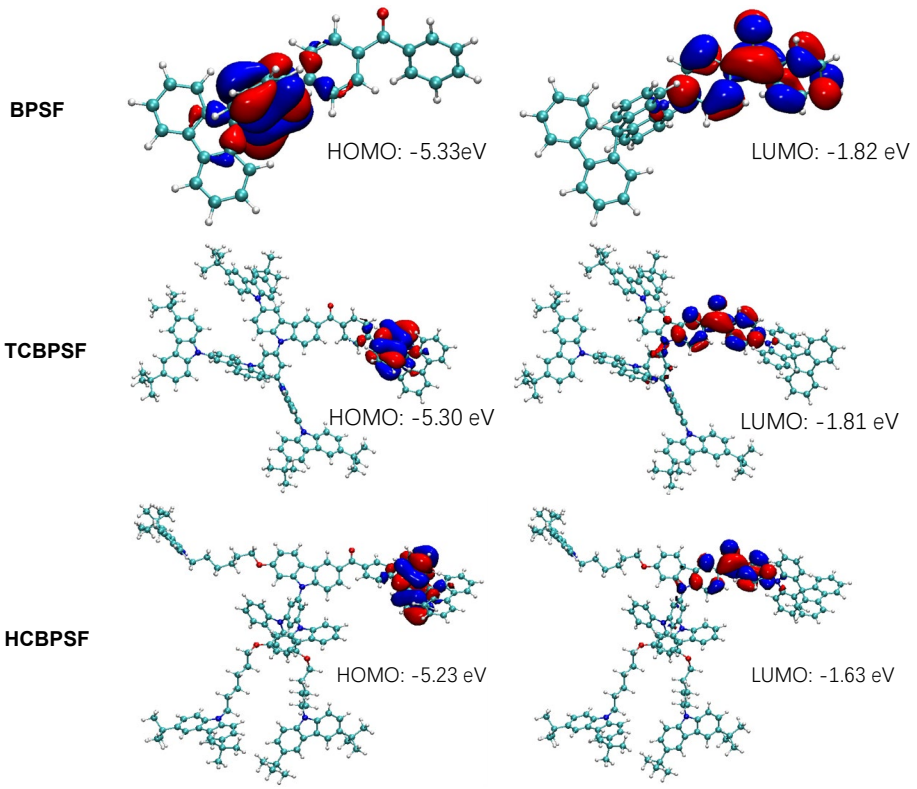

Fig. S18. The frontier molecular orbitals and energy levels of BPSF, TCBPSF, and HCBPSF.

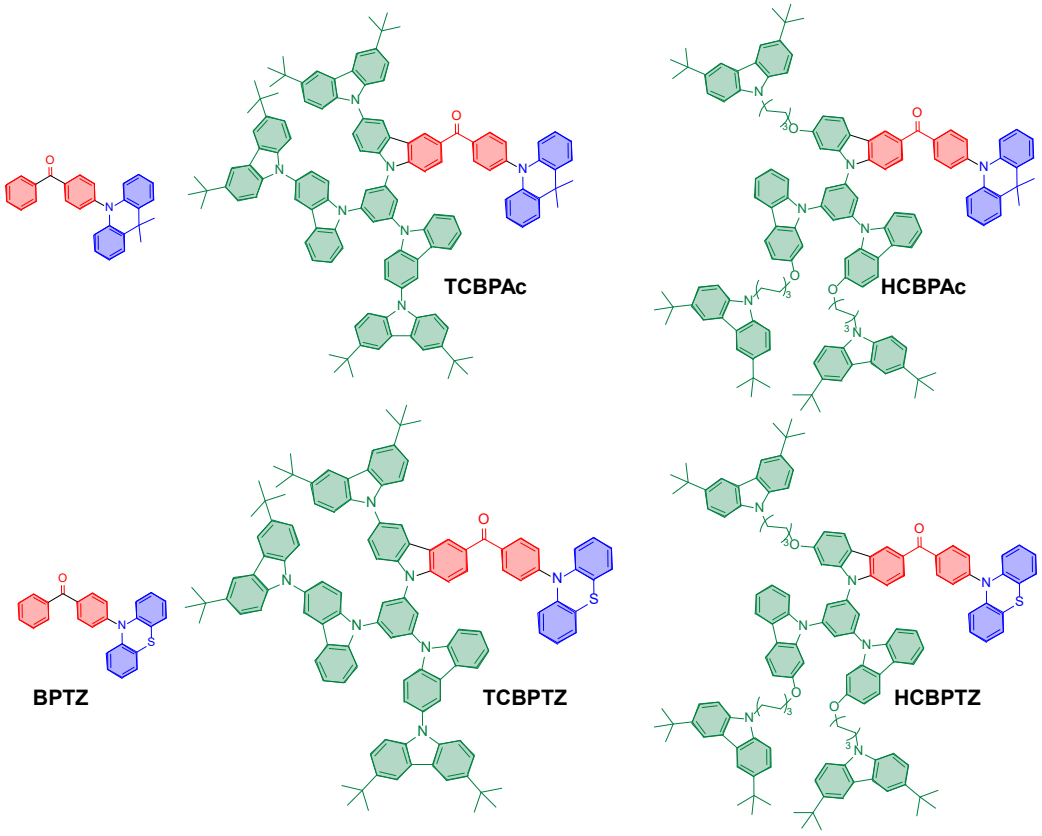

Fig. S19. Chemical structures of BPAc, TCBPAc, and HCBPAc, and BPTZ, TCBPTZ, and HCBPTZ.

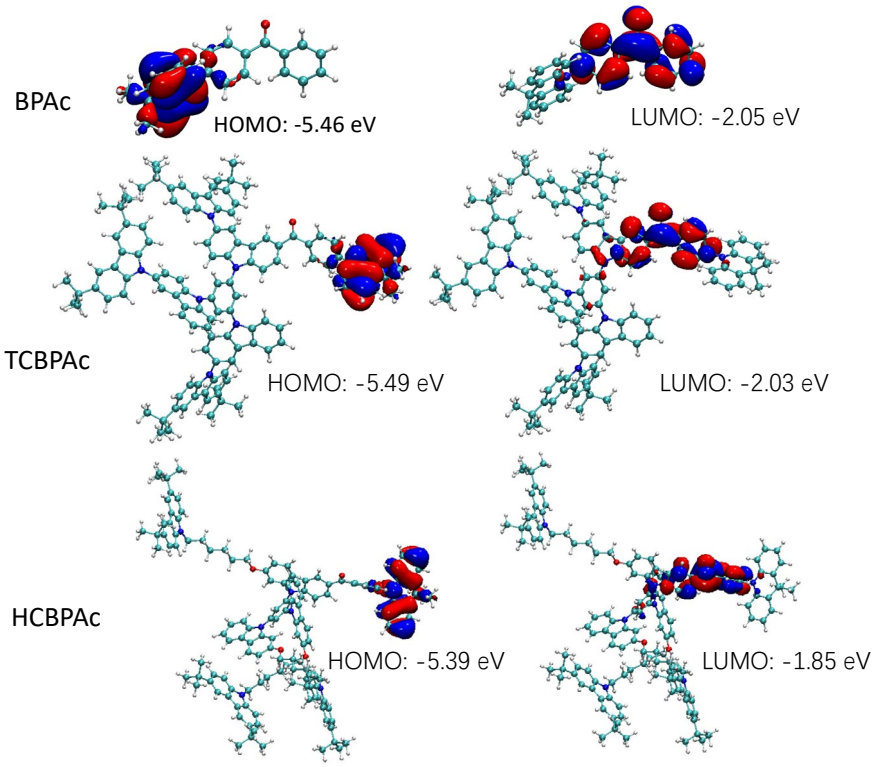

Fig. S20. The HOMOs and LUMOs of BPAc, TCBPAc, and HCBPAc.

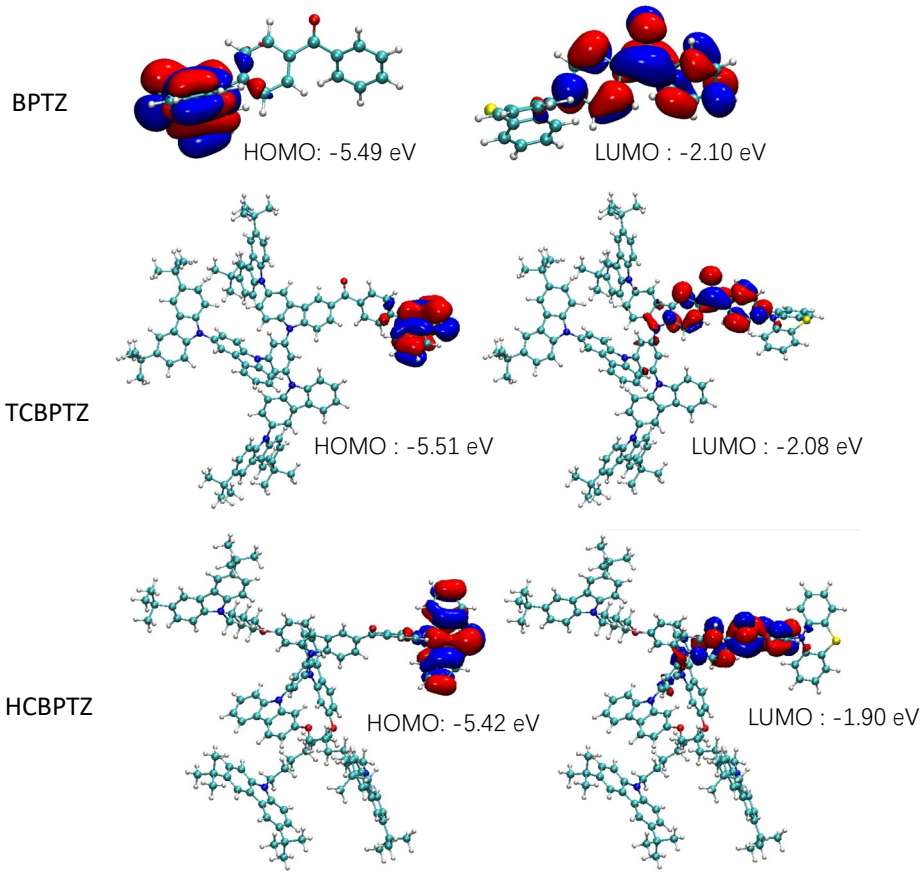

Fig. S21. The HOMOs and LUMOs of BPTZ, TCBPTZ, and HCBPTZ.

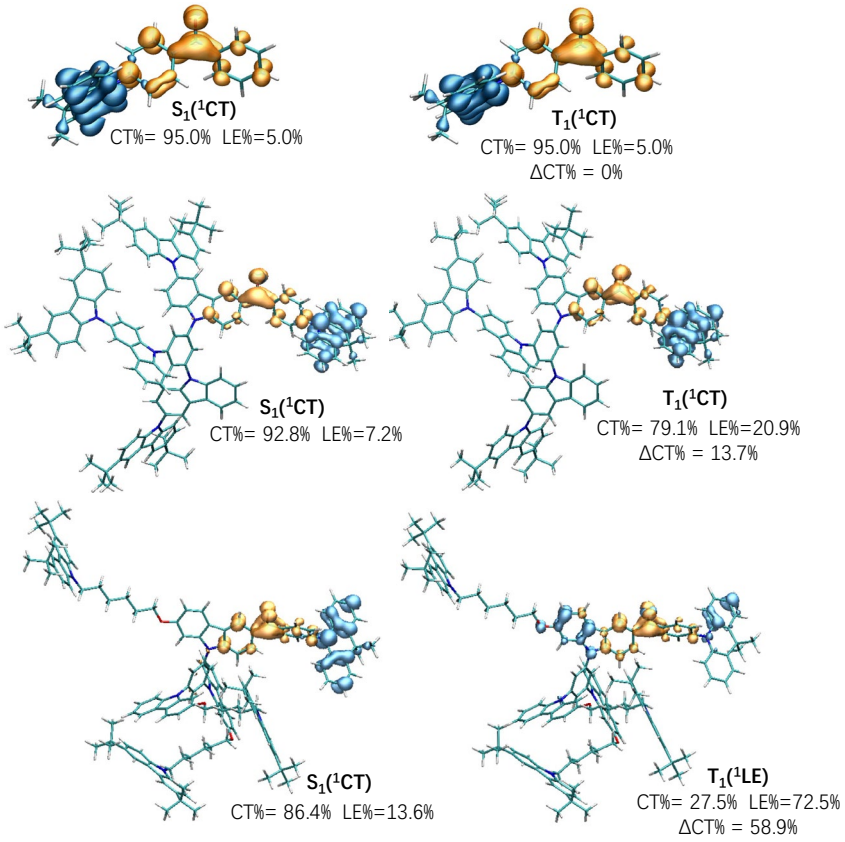

Fig. S22. The hole and electron distributions of S_1 and T_1 of BPAc, TCBPAc, and HCBPAc.

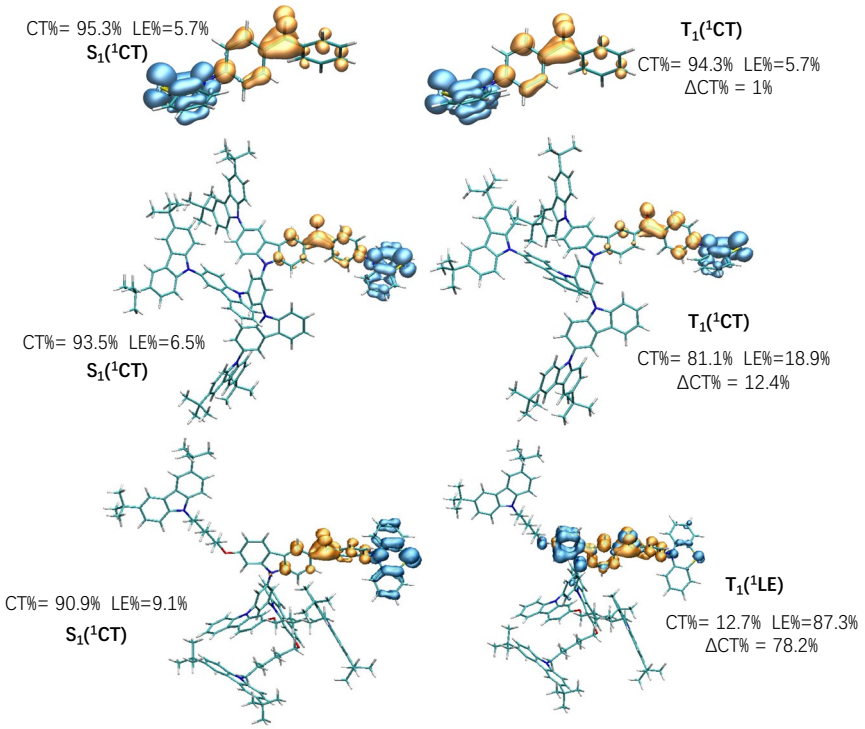

Fig. S23. The hole and electron distributions of S_1 and T_1 of BPTZ, TCBPTZ, and HCBPTZ.

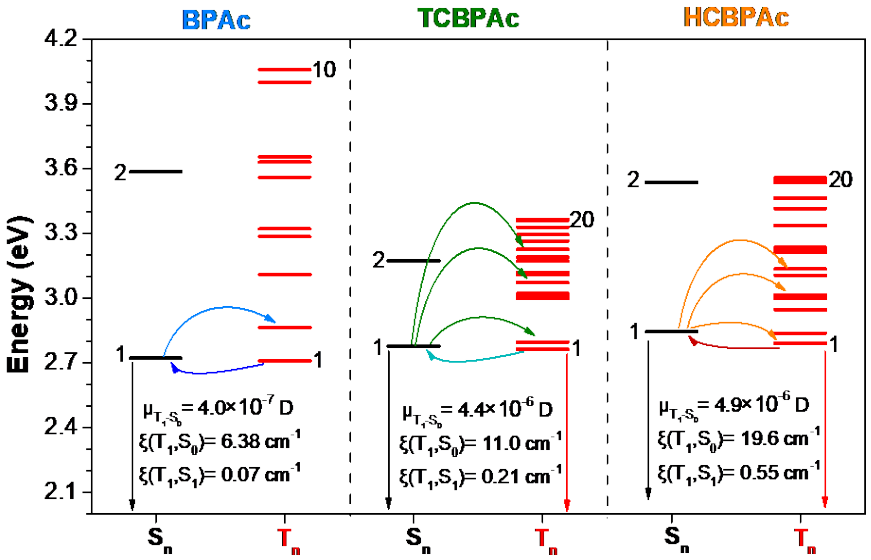

Fig. S24. The excited states, photophysical processes, triplet radiative transition ($\mu_{T_1\rightarrow S_0}$), SOC constants of BPAc, TCBPAc, and HCBPAc.

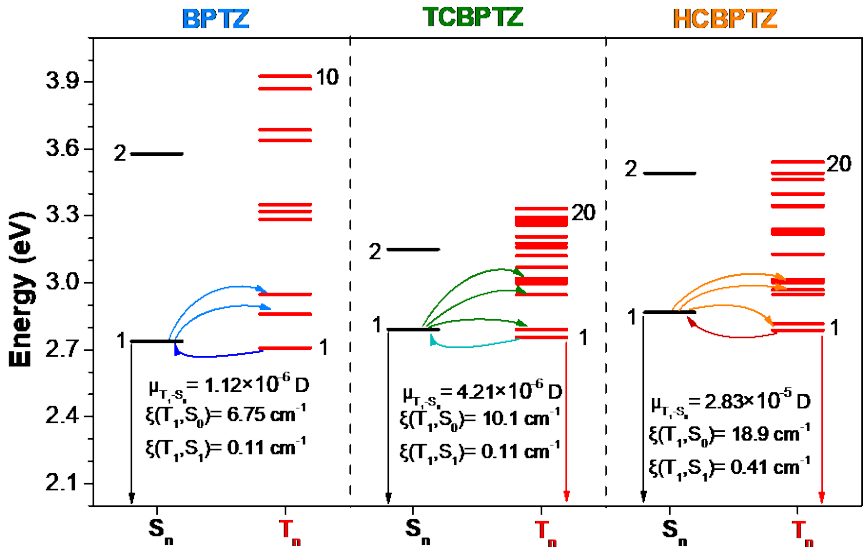

Fig. S25. The excited states, photophysical processes, triplet radiative transition ($\mu_{T_1\rightarrow S_0}$), SOC constants of BPTZ, TCBPTZ, and HCBPTZ.

Photophysical properties in films

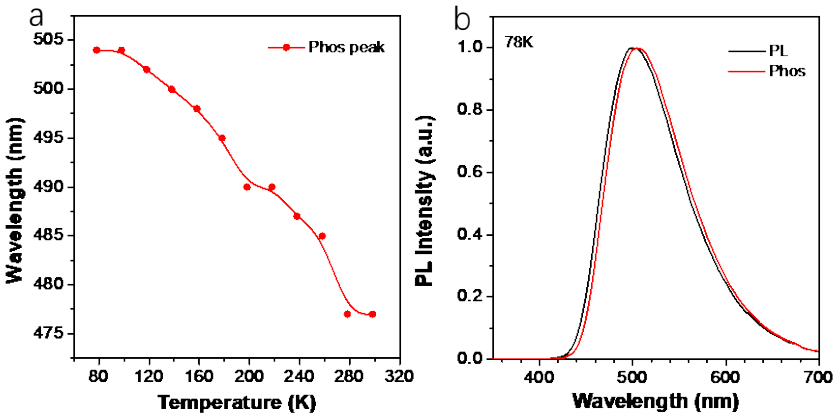

Fig. S26. (**a**) The plots of Phos peak of TCBPSF in doped PMMA films in 1 wt%. (**b**) The PL and Phos spectra of TCBPSF in doped PMMA films at 78 K.

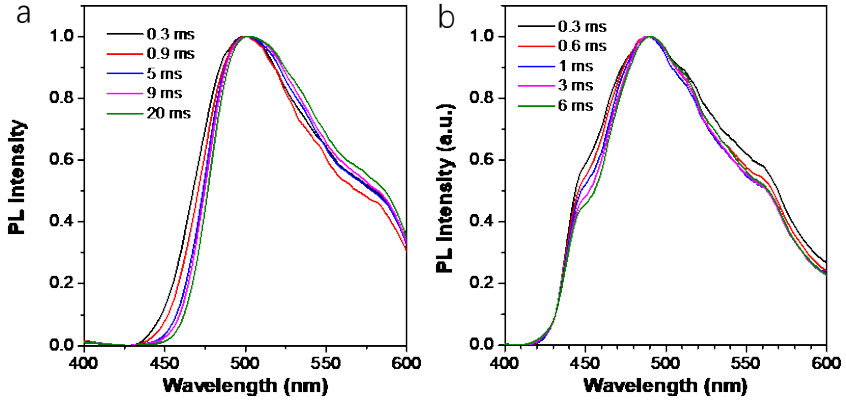

Fig. S27. Time-resolved phosphorescence spectra of TCBPSF in PMMA doped films in 1 wt% at (**a**) 78 K and (**b**) 178 K.

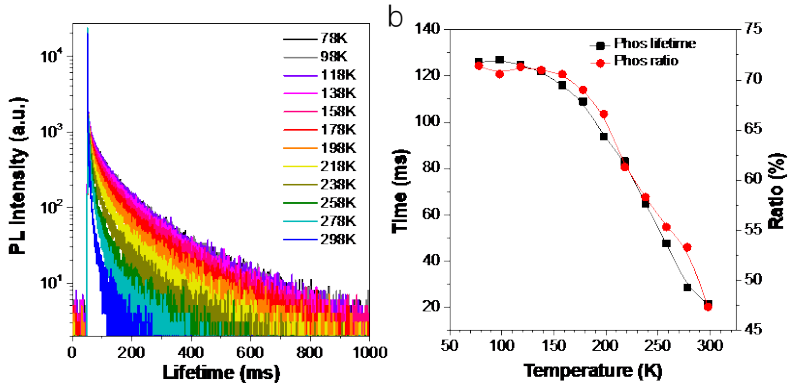

Fig. S28. (**a**) The temperature-dependent PL transient decay and (**b**) the plots of phosphorescence lifetimes and ratios of TCBPSF in PMMA doped films in 1 wt% at different temperature.

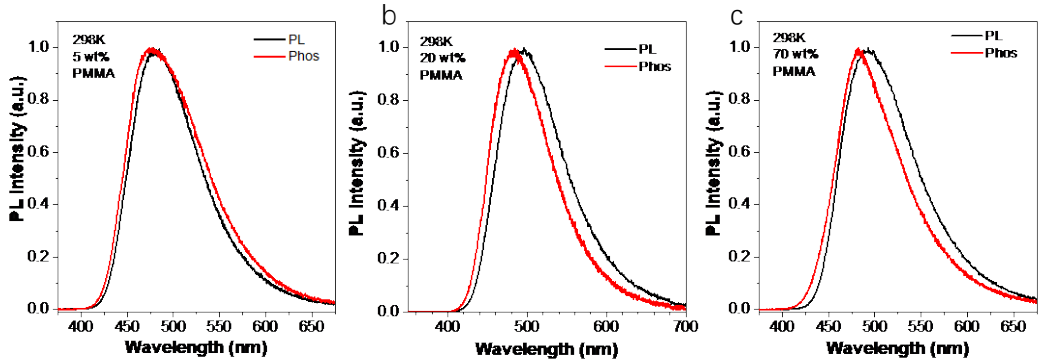

Fig. S29. The PL and Phos spectra of TCBPSF in doped PMMA films in (**a**) 5 wt%, (**b**) 20wt%, and (**c**) 70%wt% at 298 K.

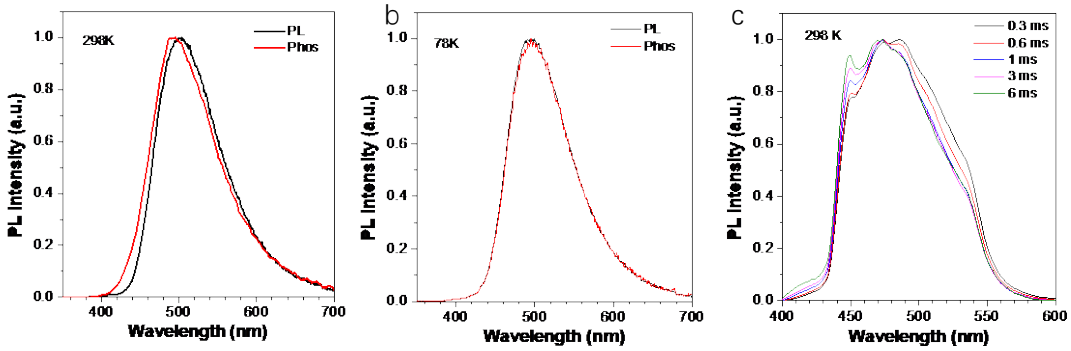

Fig. S30. The PL and Phos spectra of TCBPSF in doped PCL films in 1 wt% at (**a**) 298 K and (**b**) 78 K. (**c**) Time-resolved phosphorescence spectra of TCBPSF in PCL doped films at 298 K.

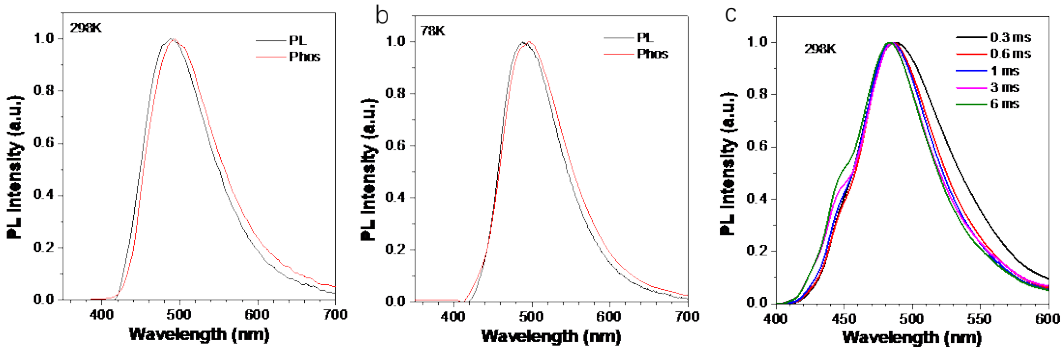

Fig. S31. The PL and phosphorescence spectra of TCBPSF in doped SBS films in 1 wt% at (**a**) 298 K and (**b**) 78 K. (**c**) Time-resolved phosphorescence spectra of TCBPSF in SBS doped films at 298 K.

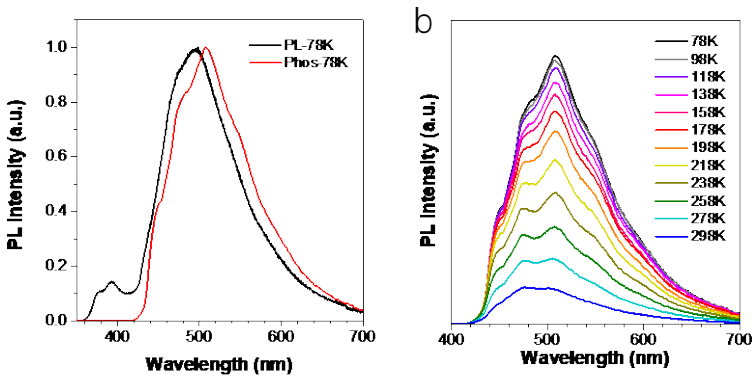

Fig. S32. (**a**) The PL and phosphorescence spectra of HCBPSF in doped PMMA films at 78 K. (**b**) Temperature-dependent phosphorescence spectra of HCBPSF in PMMA doped films at different temperatures.

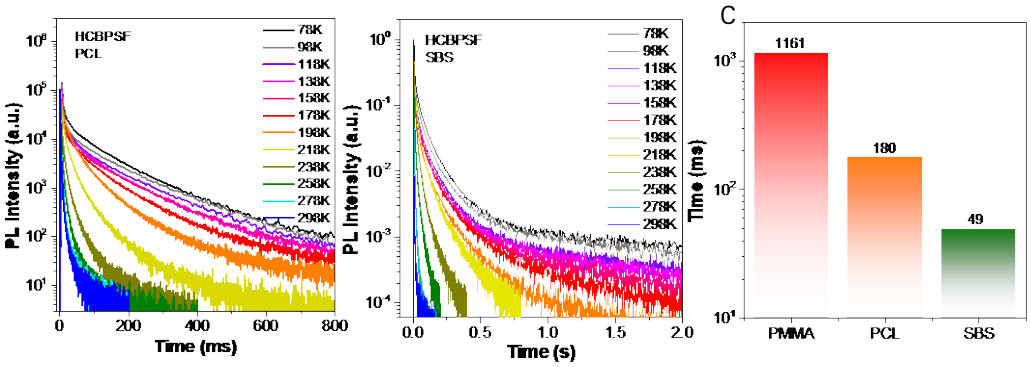

Fig. S33. The temperature-dependent PL transient decay of HCBPSF in doped PCL (**a**) and SBS (**b**) films. (**c**) The plots of phosphorescence lifetimes of HCBPSF in PMMA, PCL and SBS doped films at 298 K. The hardness of PMMA, PCL, and SBS are about 77, 53, and 47 (Shore -D), respectively.[3-5]

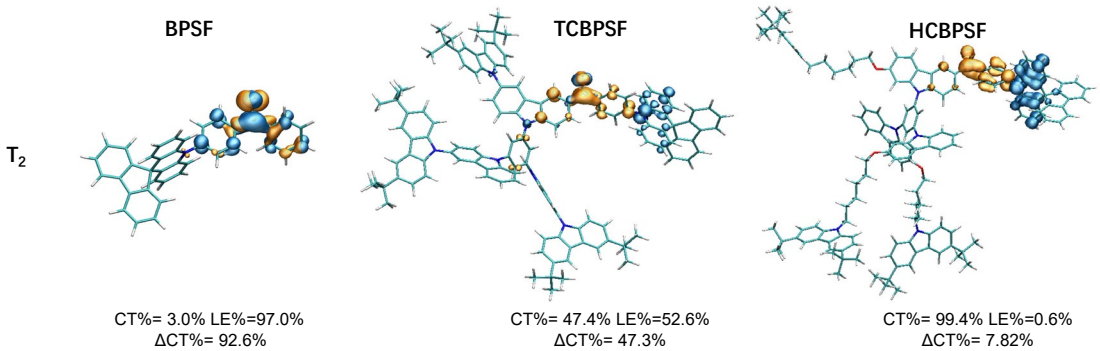

Fig. S34. The hole and electron distribution and the CT and LE proportions of T_2 of BPSF, TCBPSF, and HCBPSF.

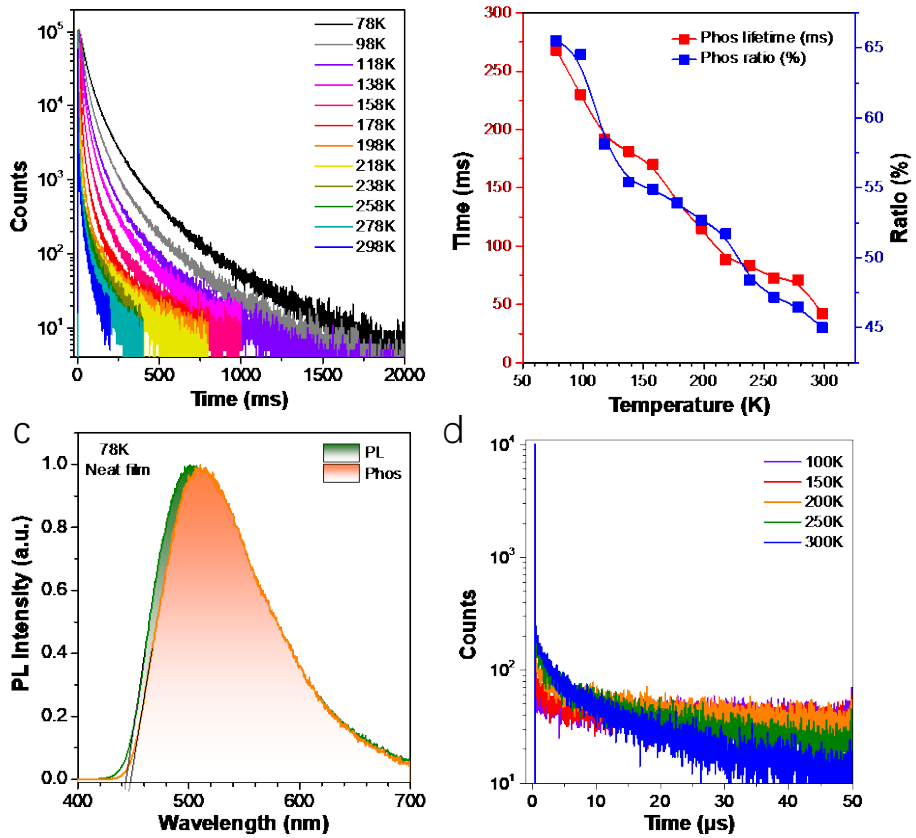

Fig. S35. The temperature-dependent PL transient decay in millisecond range (**a**) and (**b**) the plots of phosphorescence lifetimes and ratios of TCBPSF in neat films at different temperature. (**c**) The PL and Phos spectra of TCBPSF in neat films at 78 K. (**d**) The temperature-dependent PL transient decay in microsecond range of TCBPSF in neat films. The phosphorescence proportions were calculated by the component of long-lived lifetime in millisecond range. The delayed fluorescence and fluorescence proportions were calculated by the component of long-lived and short-lived lifetime in microsecond range, respectively, as shown in **Table S4**.[6]

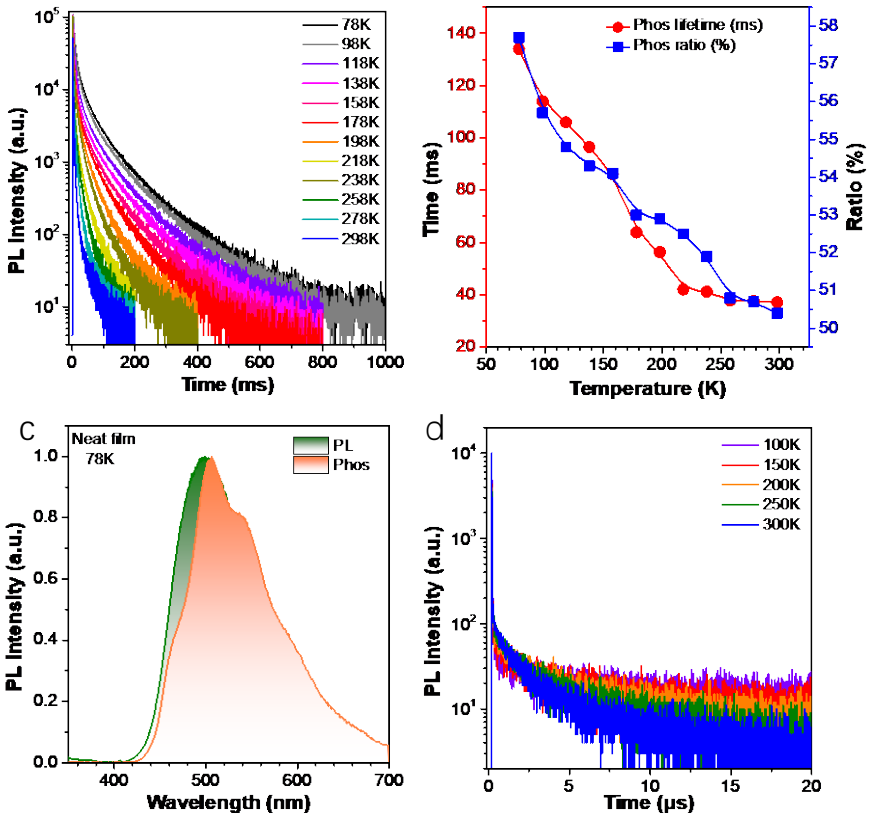

Fig. S36. The temperature-dependent PL transient decay in millisecond range (**a**) and (**b**) the plots of phosphorescence lifetimes and ratios of HCBPSF in neat films at different temperature. (**c**) The PL and phosphorescence spectra of HCBPSF in neat films at 78 K. (**d**) The temperature-dependent PL transient decay in microsecond range of TCBPSF in neat films. The phosphorescence proportions were calculated by the component of long-lived lifetime in millisecond range. The delayed fluorescence and fluorescence proportions were calculated by the component of long-lived and short-lived lifetime in microsecond range, respectively, as shown in **Table S4**.[6]

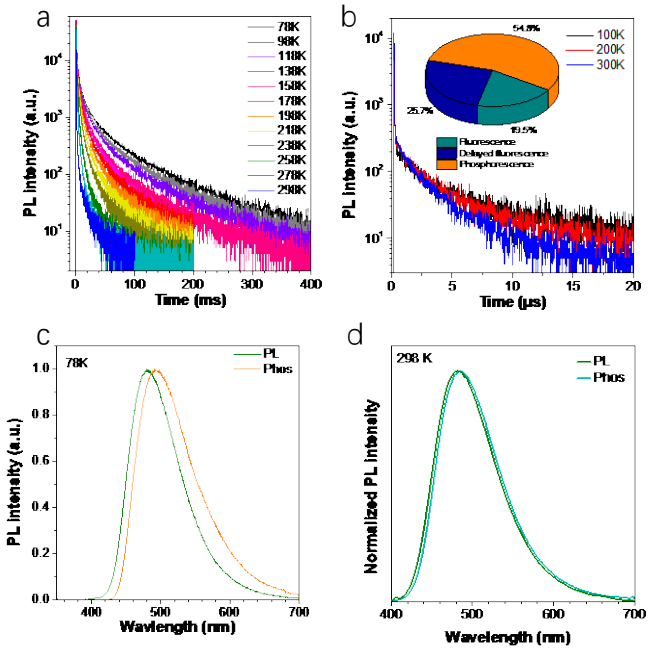

Fig. S37. The temperature-dependent PL transient decay in millisecond range (**a**) and in microsecond range (**b**) of TCBPSF in host doped films. PL and Phos spectra of TCBPSF in doped film at 78 K (**c**) and 298 K (**d**). The phosphorescence proportions were calculated by the component of long-lived lifetime in millisecond range. The delayed fluorescence and fluorescence proportions were calculated by the component of long-lived and short-lived lifetime in microsecond range, respectively, as shown in **Table S4**.[6]

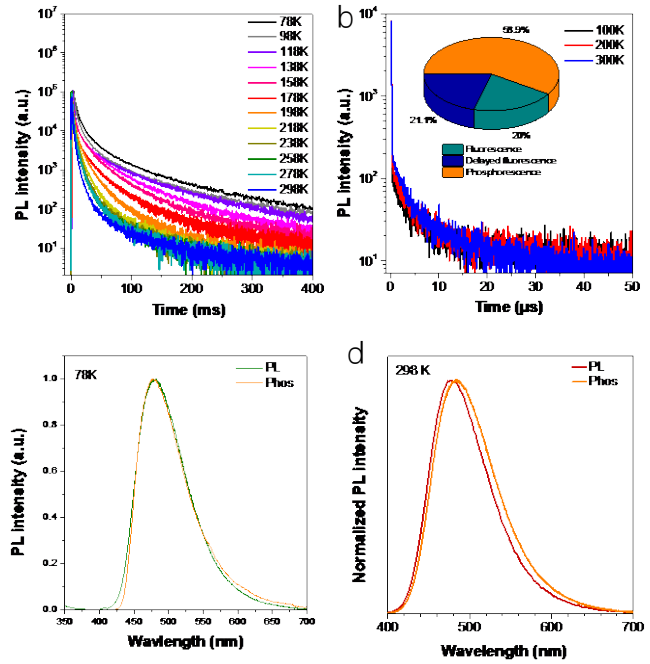

Fig. S38. The temperature-dependent PL transient decay in millisecond range (**a**) and in microsecond range (**b**) of HCBPSF in host doped films. The PL and phosphorescence spectra of HCBPSF in doped film at 78 K (**c**) and 298 K (**d**). The phosphorescence proportions were calculated by the component of long-lived lifetime in millisecond range. The delayed fluorescence and fluorescence proportions were calculated by the component of long-lived and short-lived lifetime in microsecond range, respectively, as shown in **Table S4**.[6]

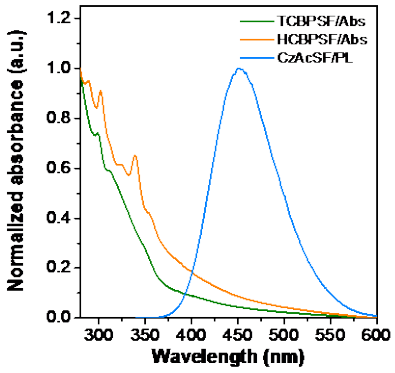

Fig. S39. The PL spectra of CzAcSF and UV-vis absorption spectra of TCBPSF and HCBPSF.

Table S4. Summary of photophysical data for BPSF, TCBPSF, and HCBPSF.

	λ_{PL}[a] (nm)	PLQY[b] (%)	ΔE_{ST}[c] (eV)	PF[d] (ns/%)	DF[e] (μs/%)	Ph[f] (ms/%)	k_{ISC}[g] (10^7 s^{-1})	k_{RISC}[h] (10^4 s^{-1})	k_F[i] (10^6 s^{-1})	k_P[j] (10^0 s^{-1})	k_{nr}[k] (10^1 s^{-1})
BPSF[7]	493	88	0.055	-/58	4.8/30	-/-	0.5	80	23	-/-	-/-
Doped BPSF[7]	491	94	0.05	-/53	5.2/41	-/-	0.14	440	22	-/-	-/-
TCBPSF	498	43	0.03	16.8/19.3	23.6/29.7	36.1/51	2.07/	1.02	4.94	6.08/	2.16
Doped TCBPSF	481	98	0.02	23.3/19.5	13.1/25.7	14.9/54.8	3.39	4.52	8.20	36.0	3.11
HCBPSF	492	31	0.03	9.23/22.6	6.9/22.0	39.4/55.4	2.60	2.15	7.59	4.36	2.10

Doped HCBPSF	478	72	0.02	16.3/20.0	3.8/21.1	37.1/58.9	3.53	9.18	8.83	11.4	1.55

[a]The peak values of PL spectra. [b]Absolute PL quantum yield determined by a calibrated integrating sphere in degassed conditions; error ± 2%. [c]Singlet-triplet energy gap in neat films and doped films at 78K. [d]The fluorescence lifetime and ratio component. [e]The delayed fluorescence lifetime and ratio component. [f]The phosphorescence lifetime and ratio component. [g]The rate constant of intersystem crossing. [h]The rate constant of reversed intersystem crossing. [i]The radiative decay rate of singlet exciton. [j]The radiative decay rate of triplet exciton. [k]The nonradiative decay rate of triplet exciton. The rate constants are calculated using the following equations: $k_{ISC} = (\varphi_{P+}\varphi_{DF})/\tau_F$, $k_{ISC} = (\varphi_{F+}\varphi_{DF})/(\tau_{DF}\times(1-\varphi_{DF}))$, $k_F = \varphi_F/\tau_F$, $k_P = \varphi_P/\tau_P$, $k_{nr} = (1-\varphi_P)/\tau_P$.

Device fabrication and characterization

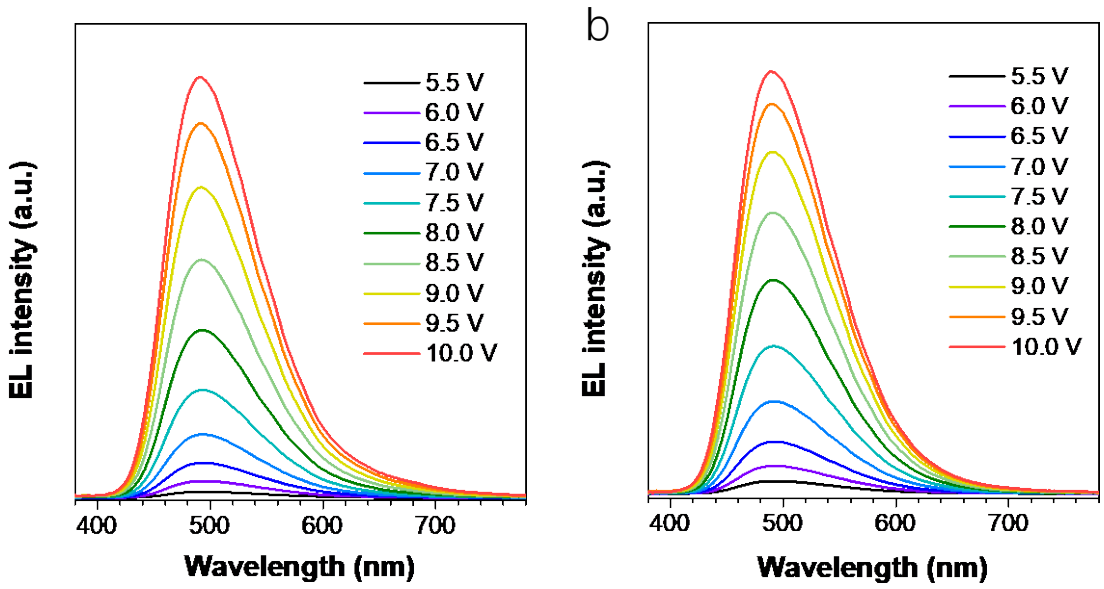

Fig. S40. The electroluminescence spectra of the devices based on CzAcSF: 10% TCBPSF (**a**) and HCBPSF (**b**) at different voltages.

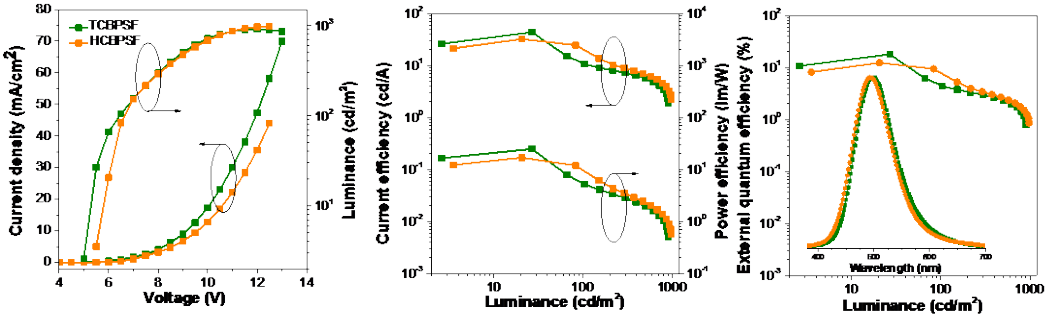

Fig. S41. (**a**) Current density-voltage-luminance curves of the devices. (**b**) Current efficiency-luminance-power efficiency curves of the devices the devices. (**c**) External quantum efficiency versus luminance curves of the devices. Inset: electroluminescence spectra of the devices. The device structure is the follows: ITO/PEDOT:PSS (70 nm)/CzAcSF: 20% Emitters (40 nm)/DPEPO (10 nm)/TmPyPB (50 nm)/Liq (1 nm)/Al (100 nm).

Table S5. EL properties of the solution-processed devices based on CzAcSF: 20% emitters.

	V_{on} (V)	**L_{max} (cd/m^2)**	**CE_{max} (cd/A)**	**PE_{max} (lm/W)**	**EQE_{max} (%)**	**EL peak (nm)**	**CIE (x,y)**
TCBPSF (20%)	5.0	905	43.4	24.8	17.9	498	0.19. 0.39
HCBPSF (20%)	5.5	983	32.2	16.8	12.3	492	0.19. 0.36

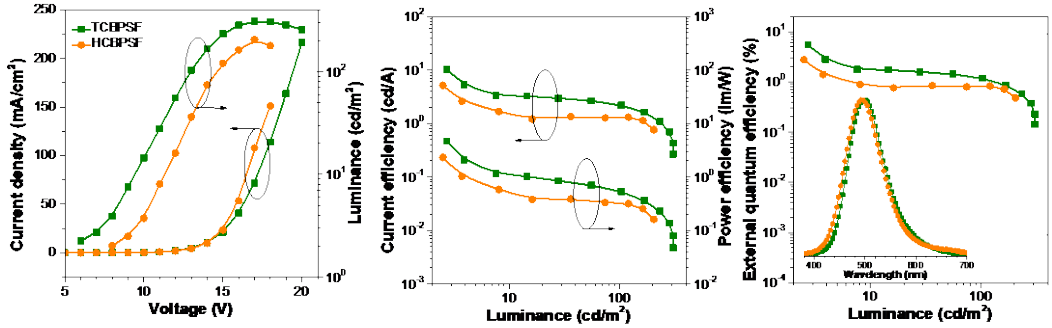

Fig. S42. (**a**) Current density-voltage-luminance curves of the devices. (**b**) Current efficiency-luminance-power efficiency curves of the devices the devices. (**c**) External quantum efficiency versus luminance curves of the devices. Inset: electroluminescence spectra of the devices. The device structure is the follows: ITO/PEDOT:PSS (70 nm)/ Emitters (40 nm)/DPEPO (10 nm)/TmPyPB (50 nm)/Liq (1 nm)/Al (100 nm).

Table S6. EL properties of the solution-processed non-doped devices.

	V_{on} (V)	**L_{max} (cd/m²)**	**CE_{max} (cd/A)**	**PE_{max} (lm/W)**	**EQE_{max} (%)**	**EL peak (nm)**	**CIE (x,y)**
TCBPSF	6	308	10.3	4.6	5.5	498	0.20. 0.40
HCBPSF	8	205	5.2	2.3	2.8	492	0.19. 0.36

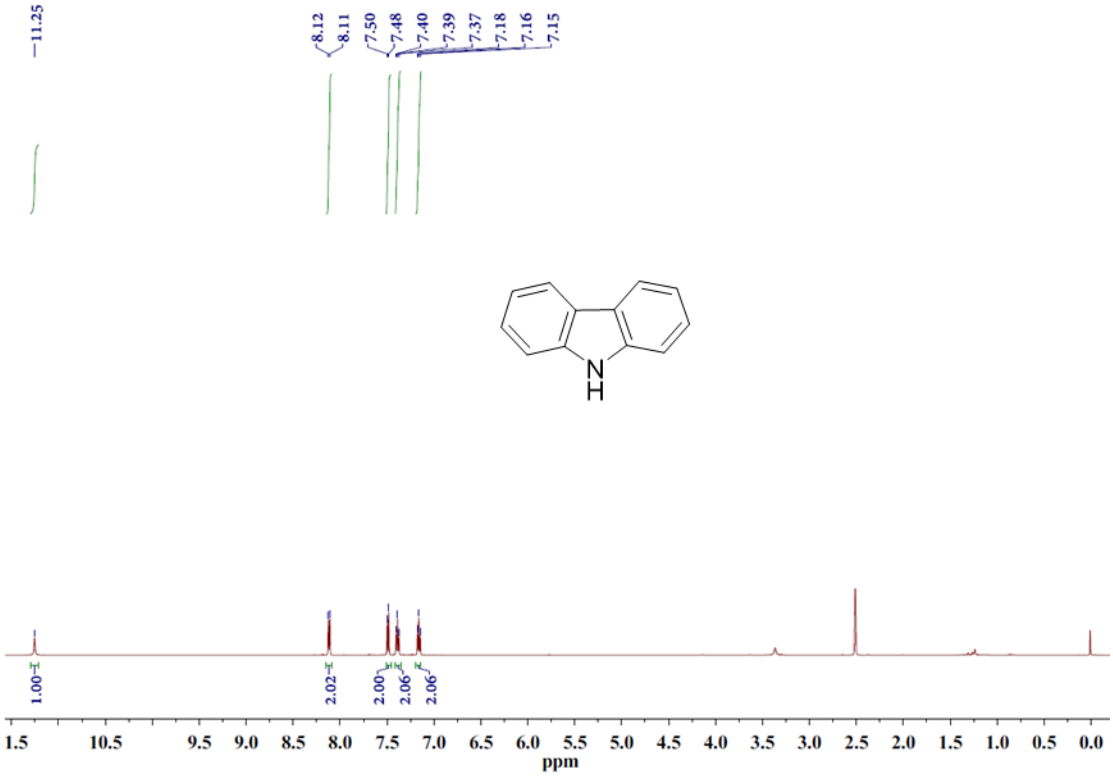

Fig. S43. ^{1}H NMR spectra of **1**.

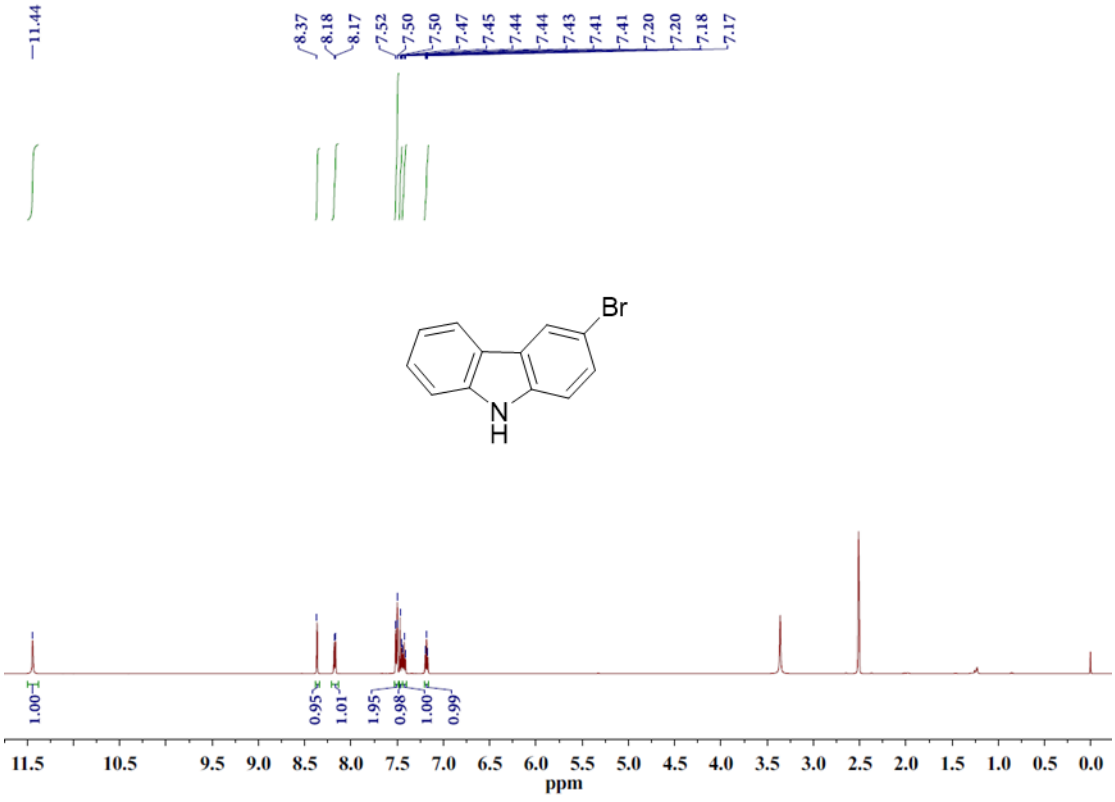

Fig. S44. ^{1}H NMR spectra of **2**.

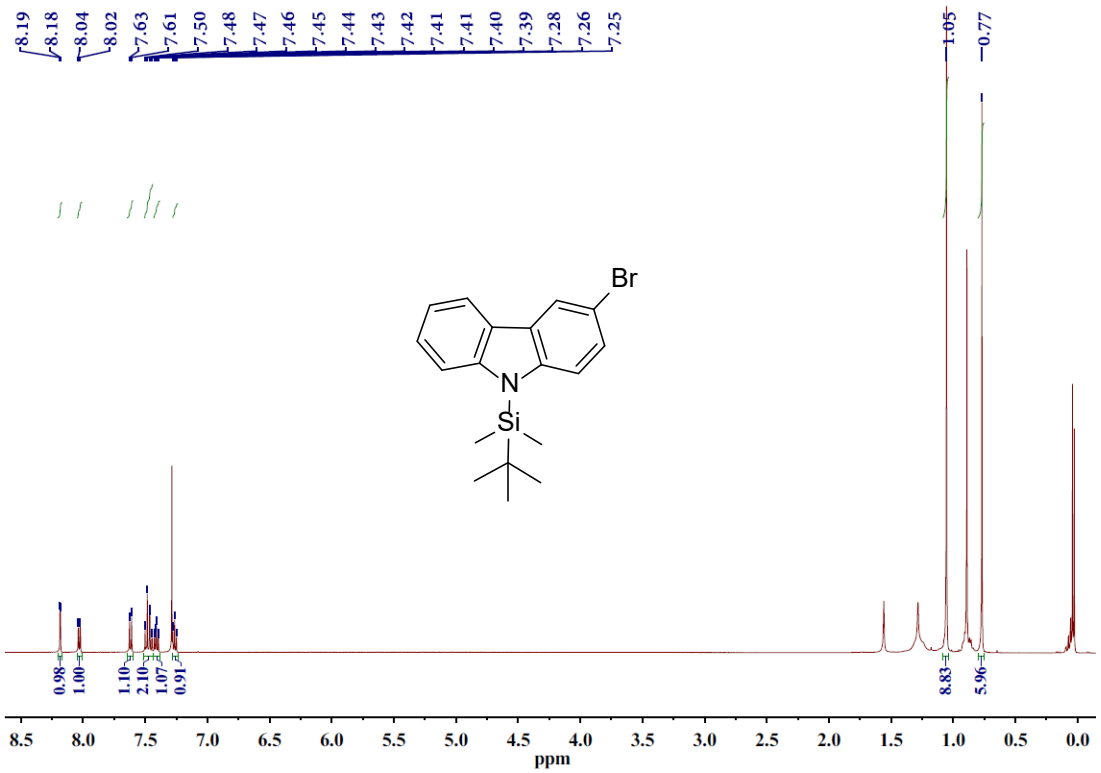

Fig. S45. ^{1}H NMR spectra of **3**.

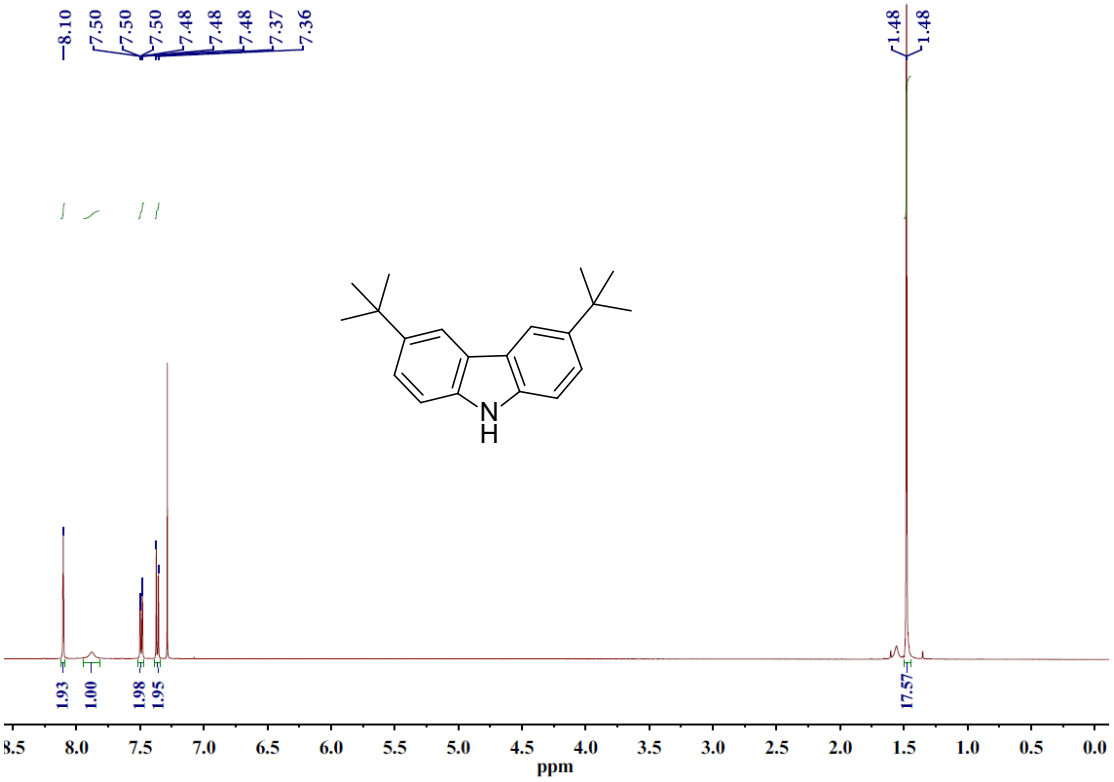

Fig. S46. ^{1}H NMR spectra of **4**.

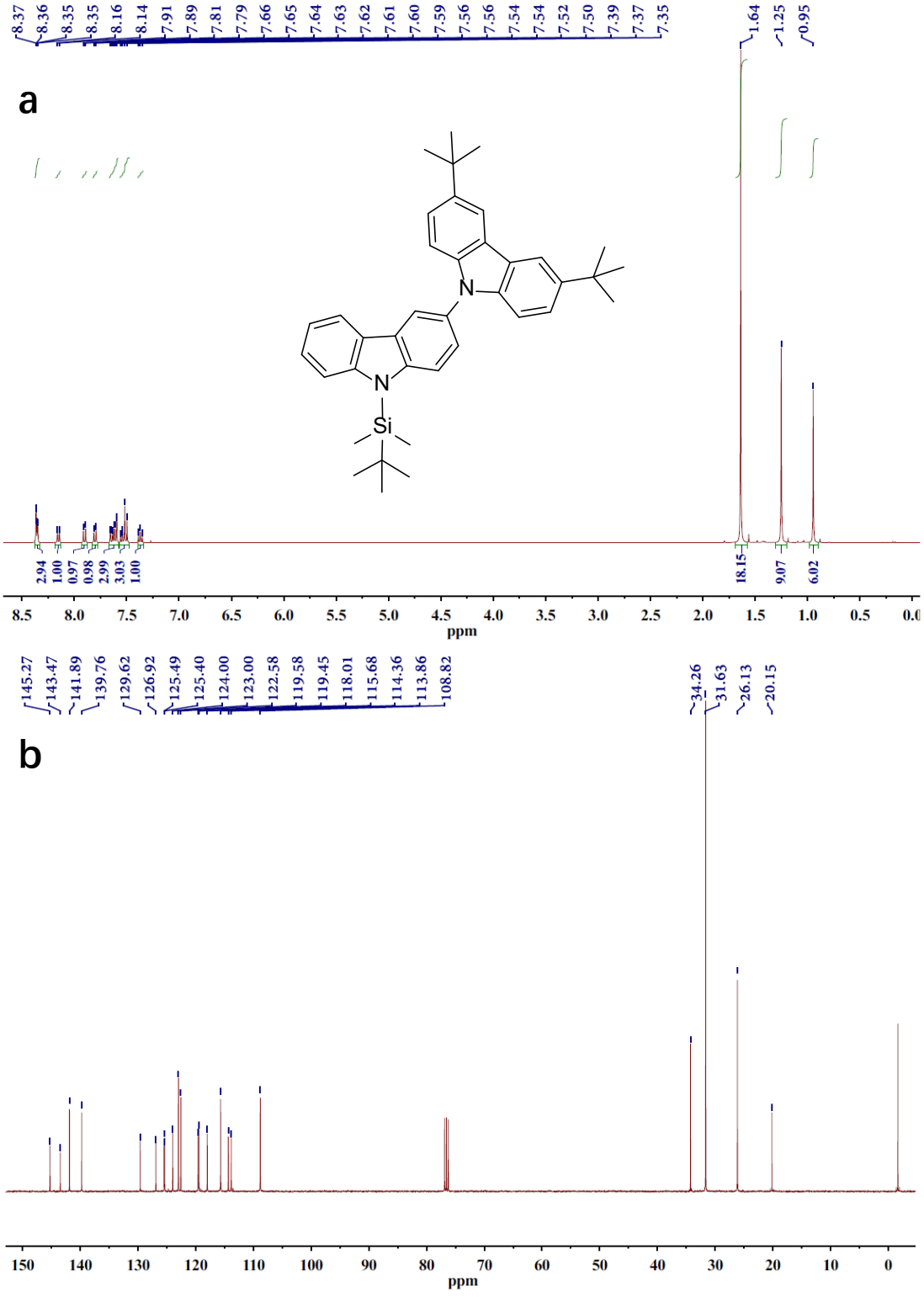

Fig. S47. a ^{1}H NMR and **b** ^{13}C NMR spectra of **5**.

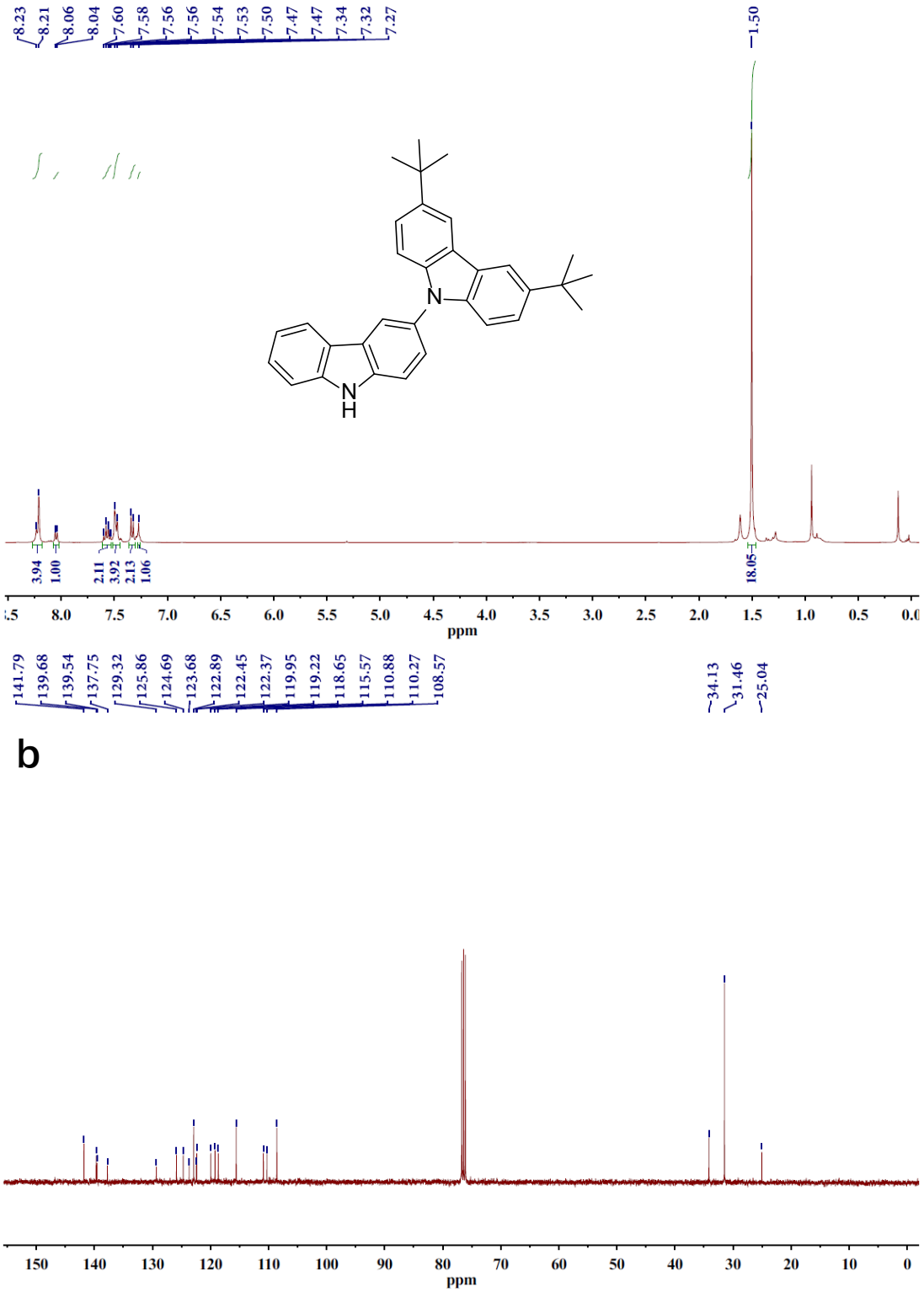

Fig. S48. (**a**) ^{1}H and (**b**) ^{13}C NMR spectra of **6**.

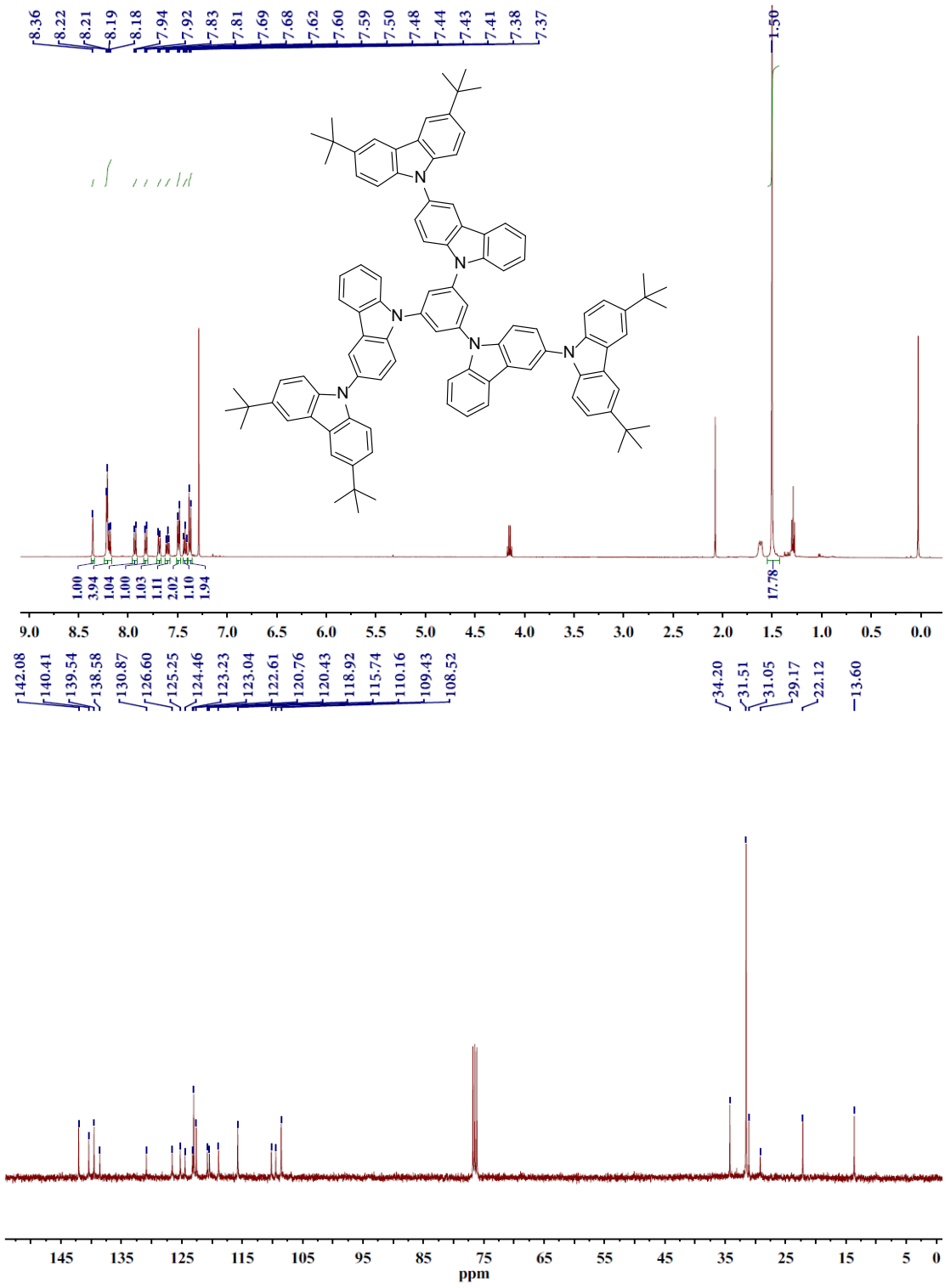

Fig. S49. (**a**) ^{1}H and (**b**) ^{13}C NMR spectra of **7**.

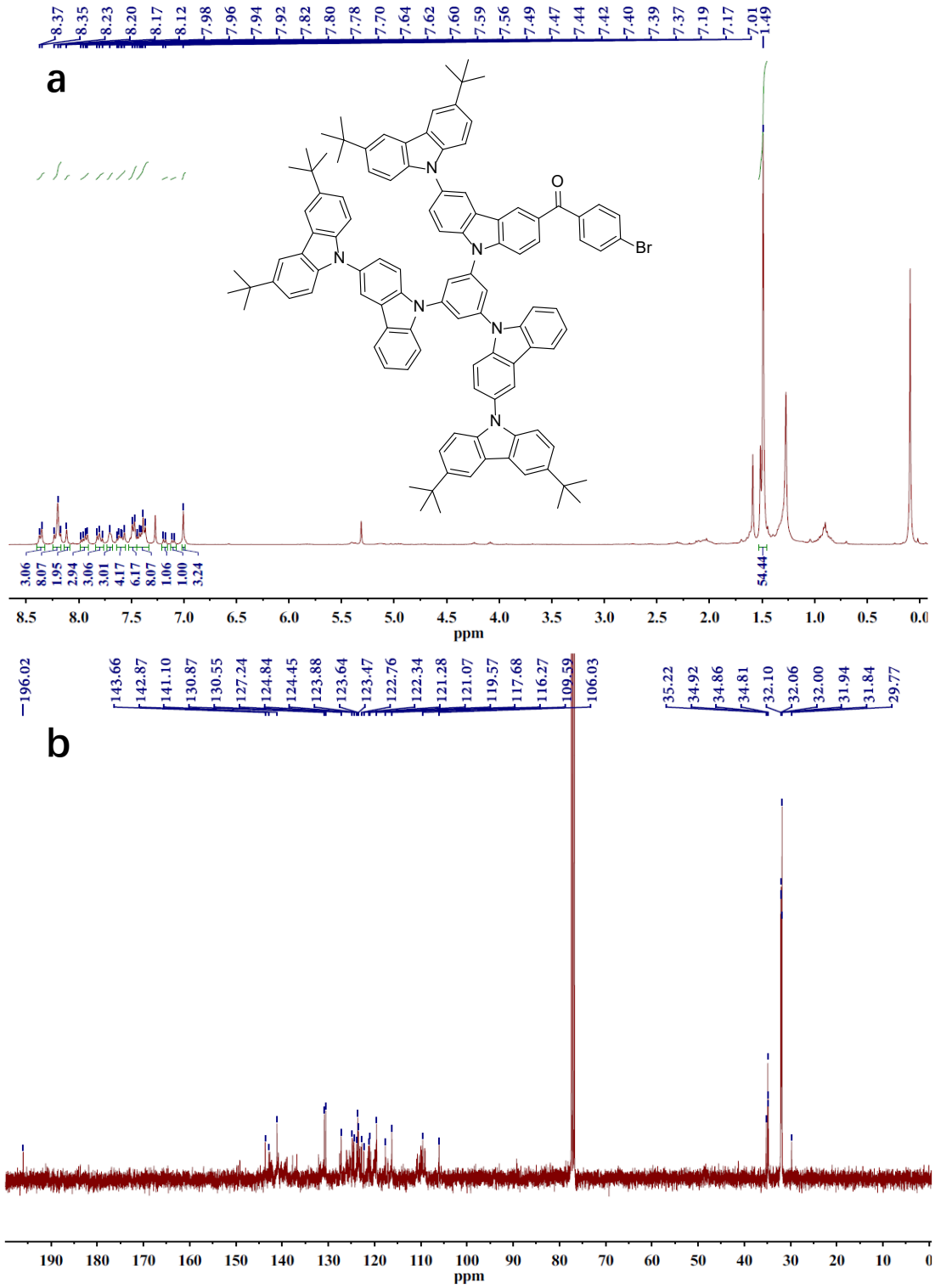

Fig. S50. (**a**) ^{1}H and (**b**) ^{13}C NMR spectra of **8**.

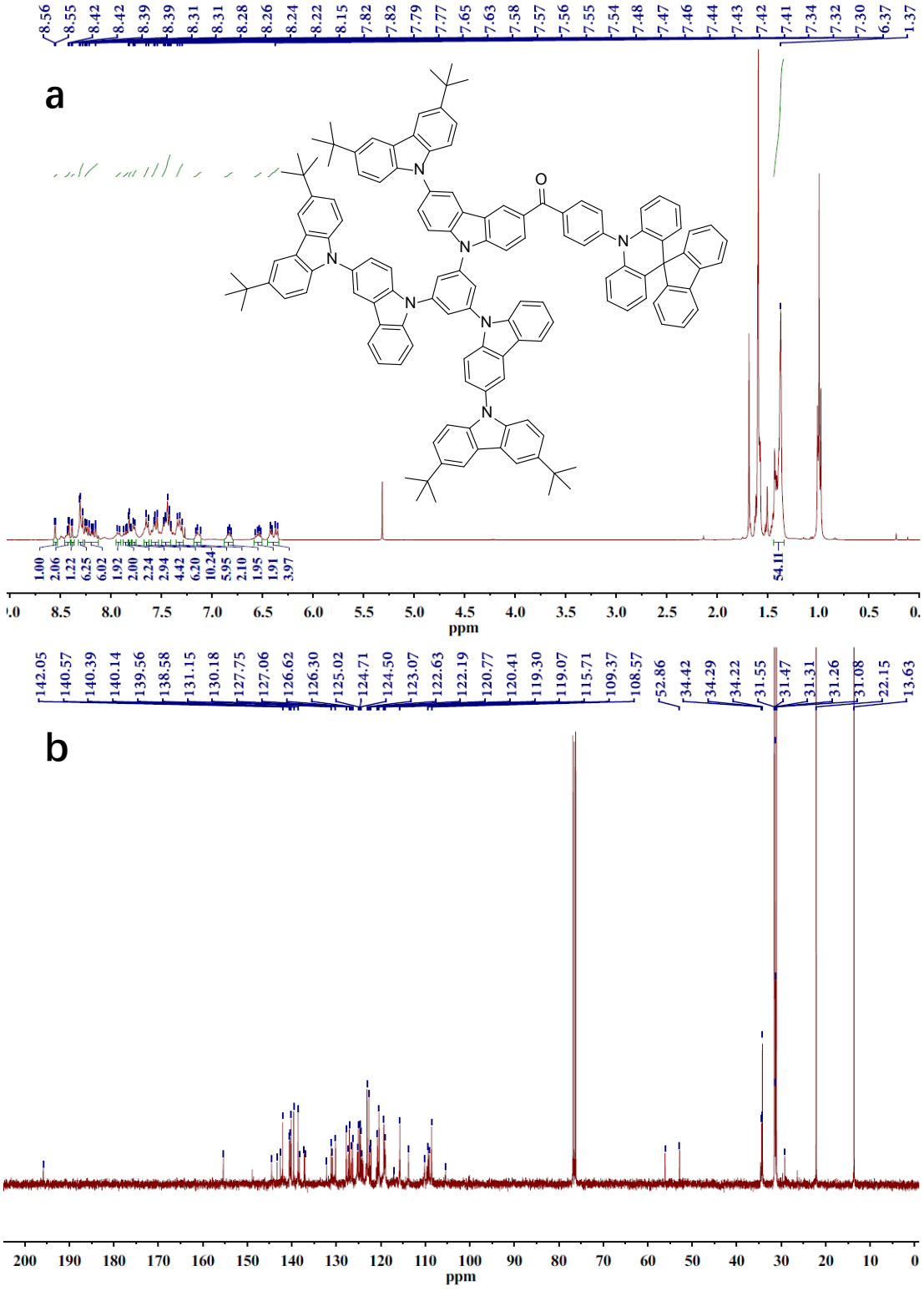

Fig. S51. (**a**) ^{1}H and (**b**) ^{13}C NMR spectra of **TCBPSF**.

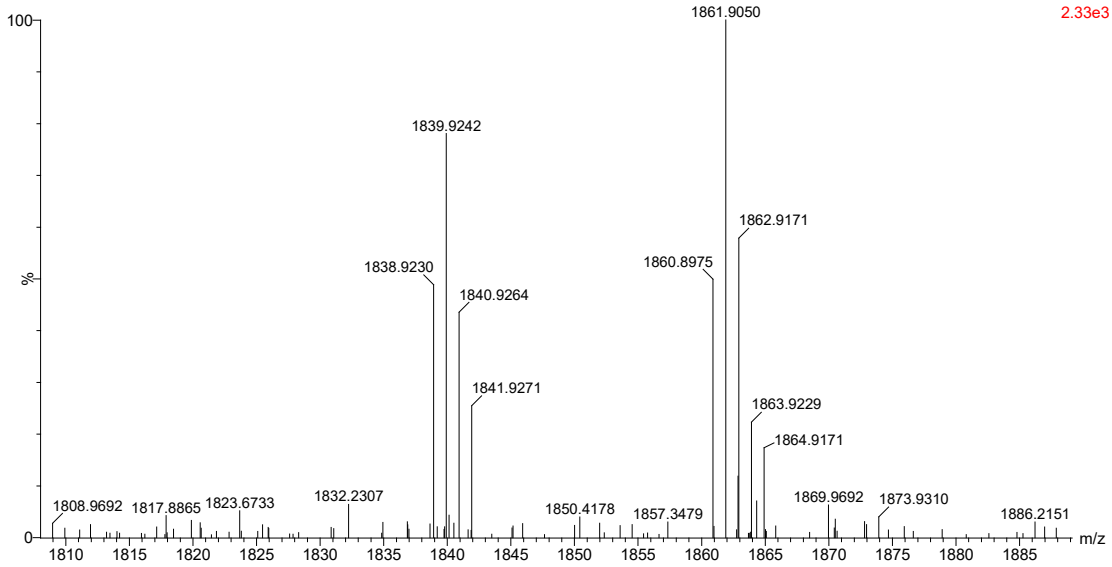

Fig. S52. MALDI-TOF MS spectra of **TCBPSF**.

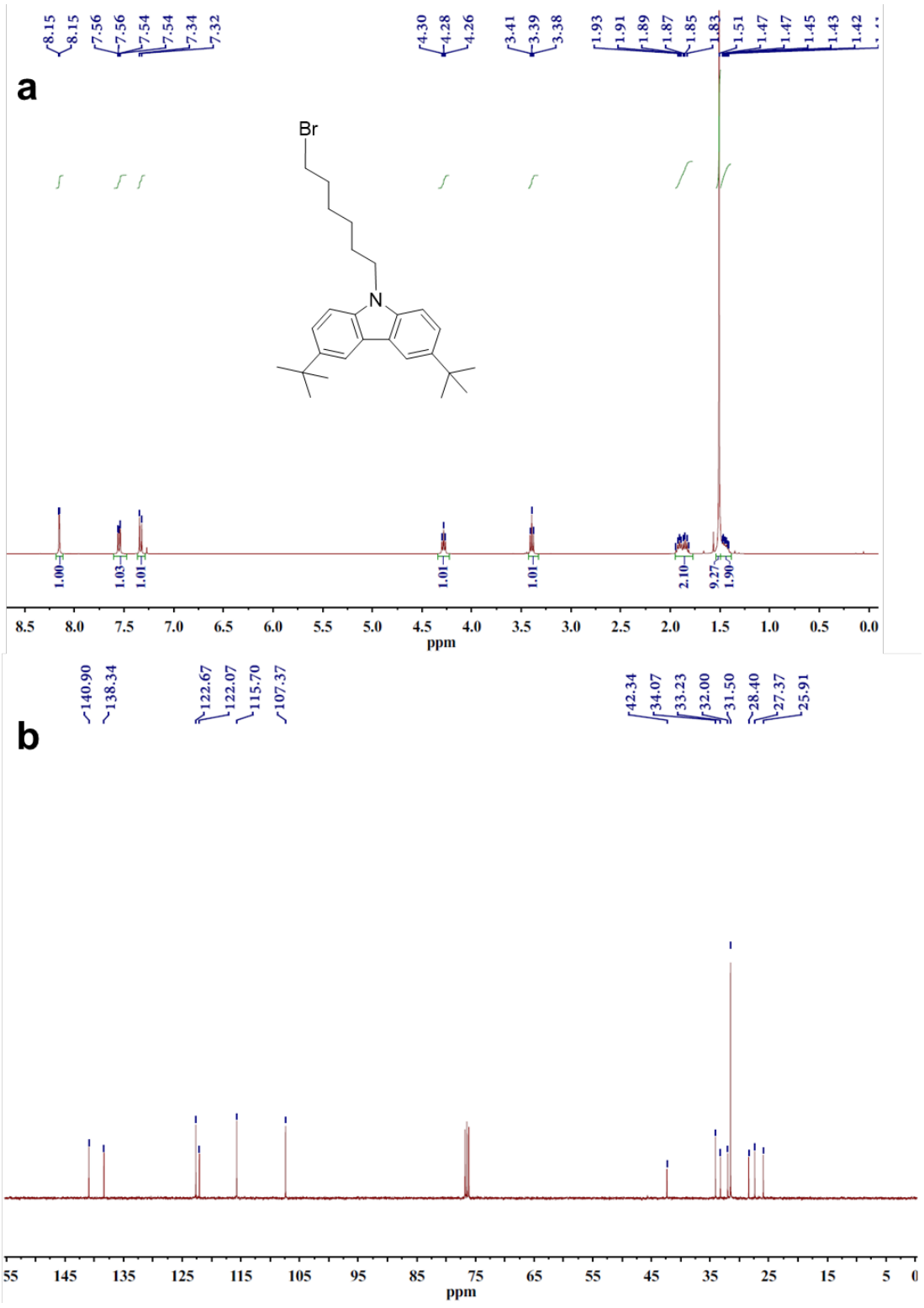

Fig. S53. (**a**) ^{1}H and (**b**) ^{13}C NMR spectra of **9**.

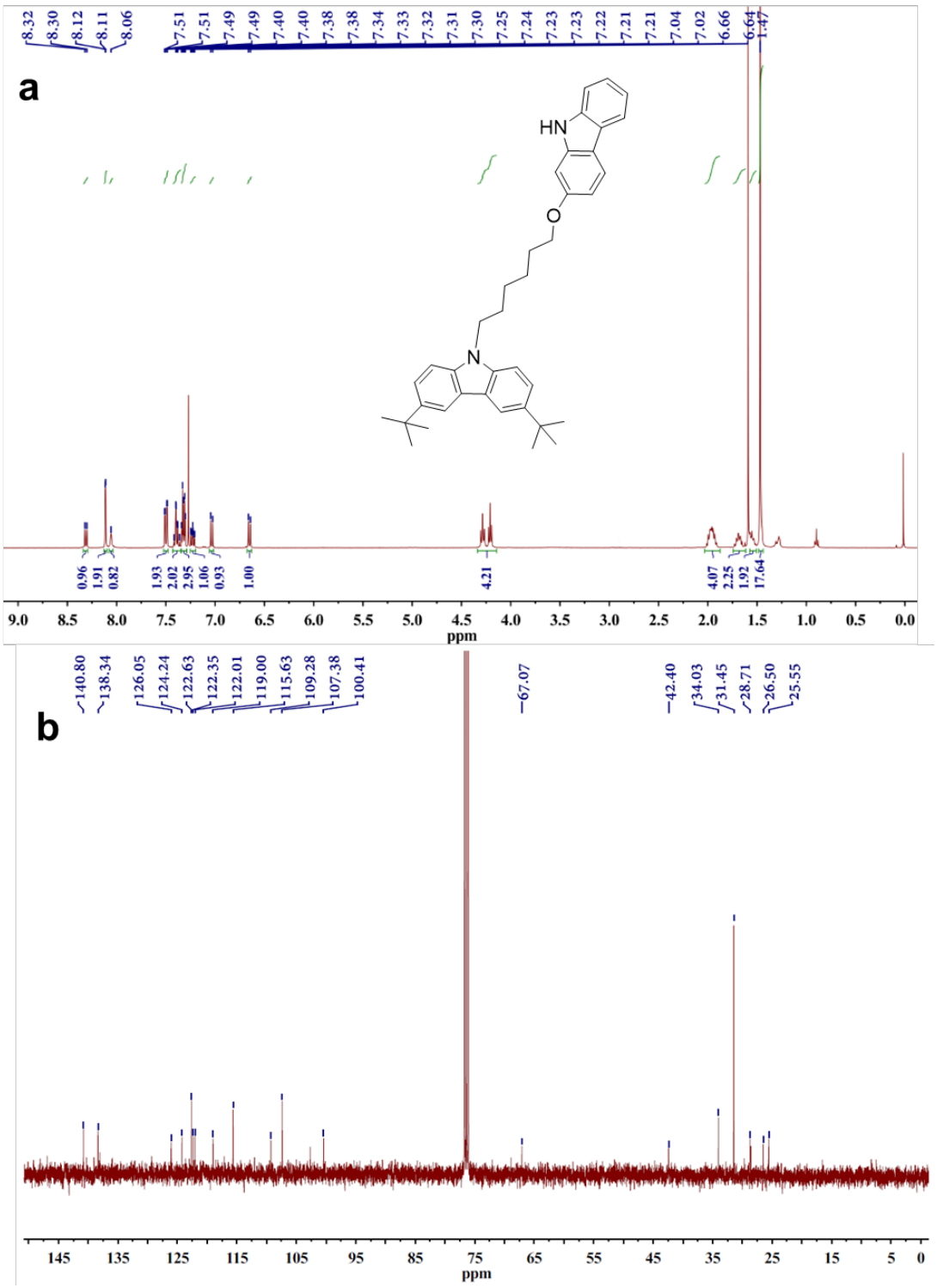

Fig. S54. (**a**) ^{1}H NMR and (**b**) ^{13}C NMR spectra of **10**.

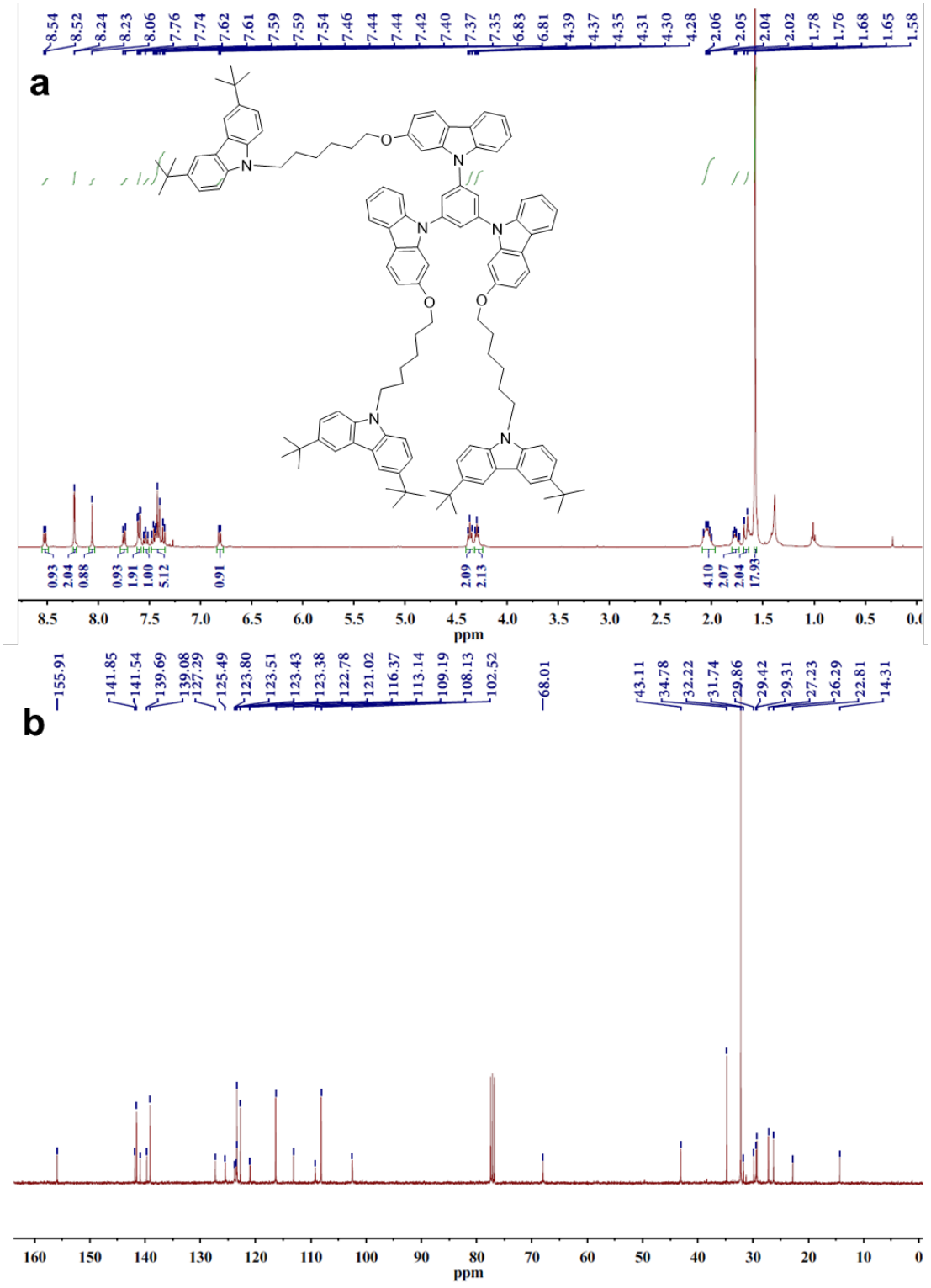

Fig. S55. (**a**) ^{1}H NMR and (**b**) ^{13}C NMR spectra of **11**.

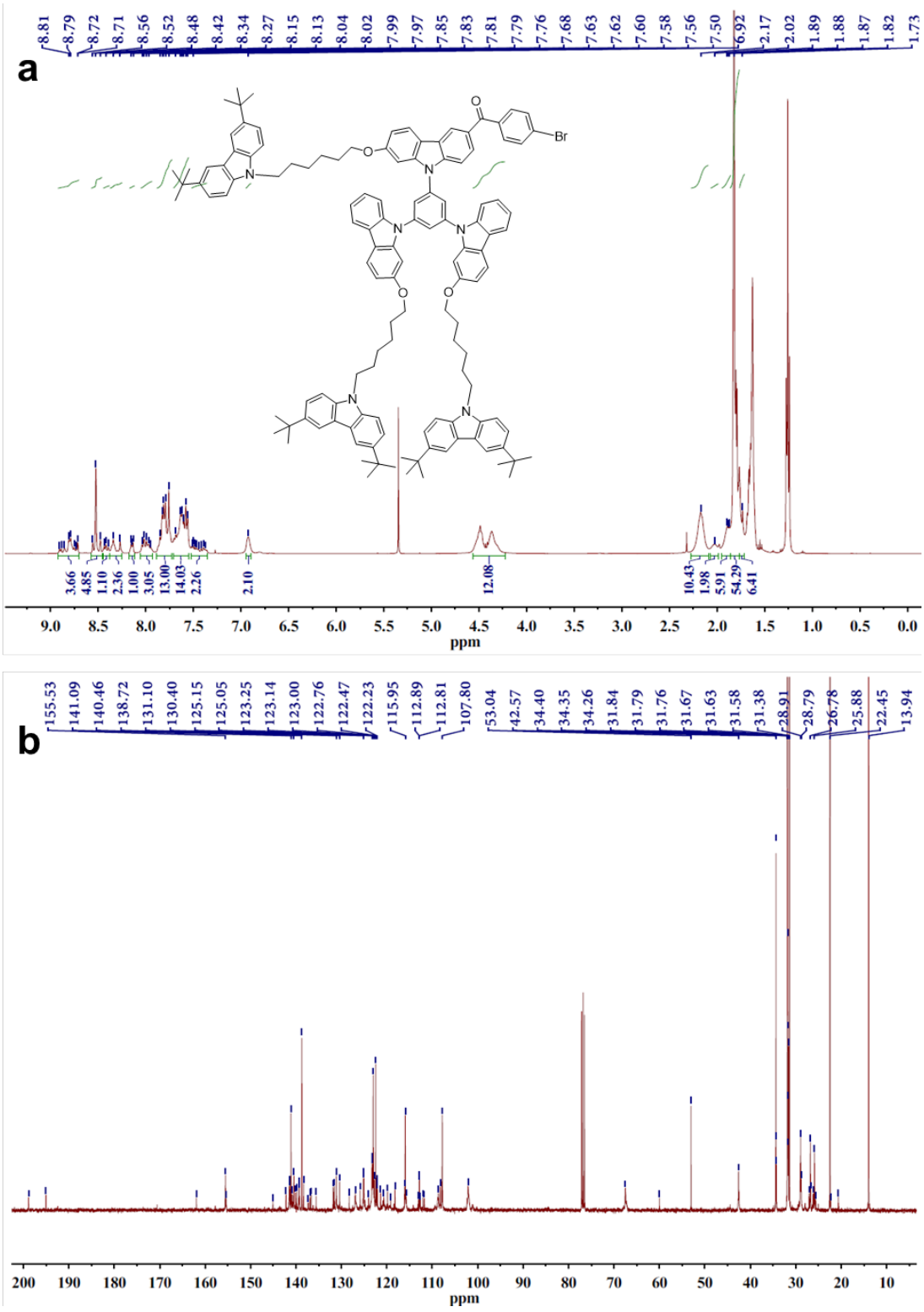

Fig. S56. (**a**) ^{1}H NMR and (**b**) ^{13}C NMR spectra of **12**.

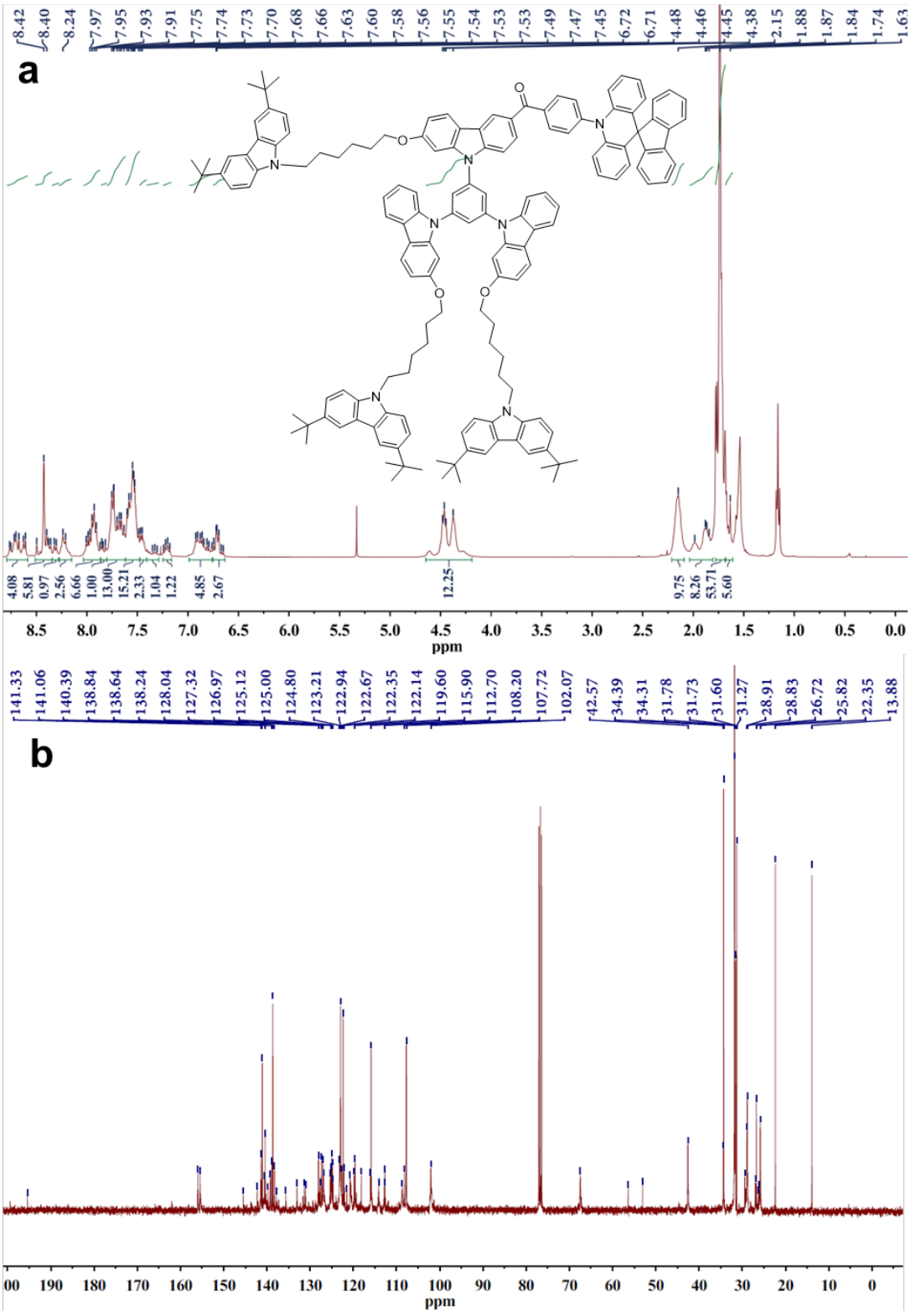

Fig. S57. (**a**) ^{1}H NMR and (**b**) ^{13}C NMR spectra of **HCBPSF**.

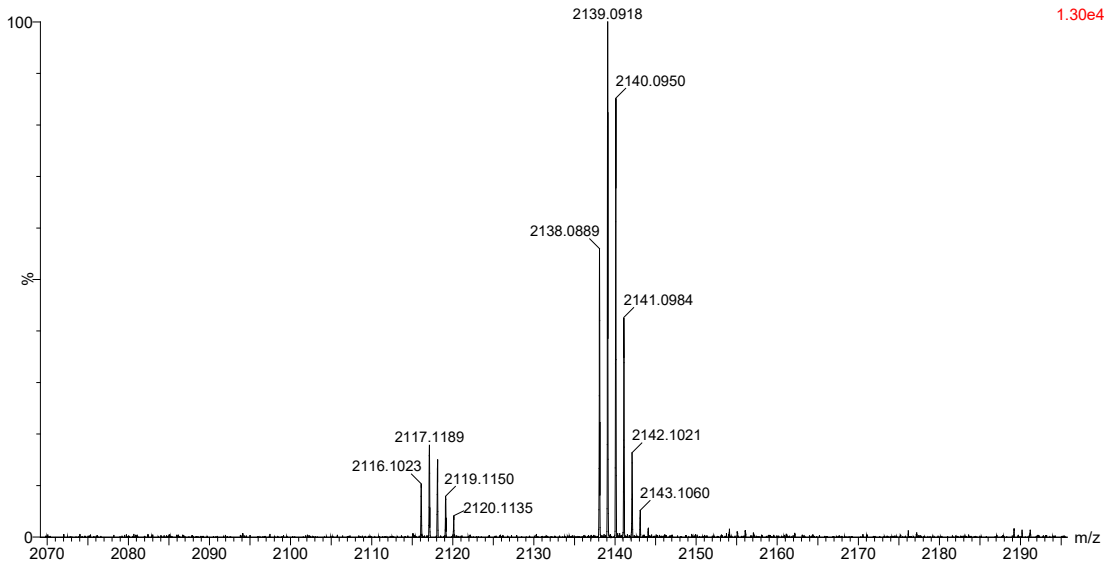

Fig. S58. MALDI-TOF MS spectra of **HCBPSF**.

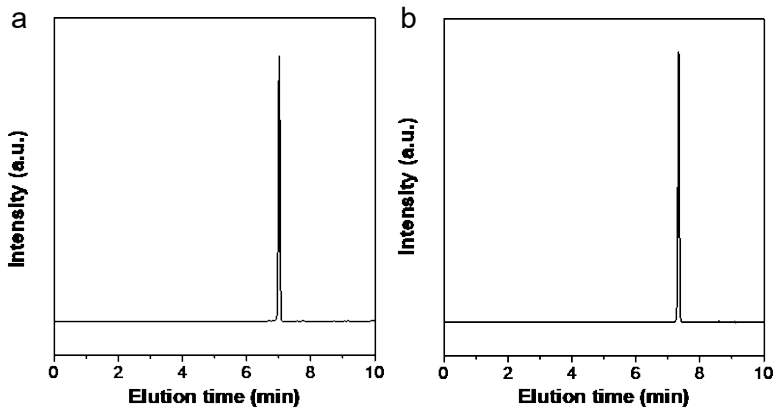

Fig. S59. High-performance liquid chromatogram of the TCBPSF (**a**) HCBPSF (**b**) in acetonitrile/water mixtures.

References

1. Qian, C. *et al.* Carbazole&benzoindole-based purely organic phosphors: a comprehensive phosphorescence mechanism, tunable lifetime and an advanced encryption system. *J. Mater. Chem. C* **9**, 14294-14302 (2021).
2. Wu, J. *et al.* Novel 2,1,3-benzothiadiazole derivatives used as selective fluorescent and colorimetric sensors for fluoride ion. *Dyes and Pigments* **124**, 268-276 (2016).
3. E. Salih, S., K. Oleiwi, J. & Mohammed.T, A. Investigation of Hardness and Flexural Properties of PMMA Nano Composites and PMMA Hybrids Nano

Composites Reinforced by Different Nano Particles Materials used in Dental Applications. *Eng. Technol. J.* **34**, 2838-2853 (2016).

4. Pavon, C., Aldas, M., López-Martínez, J. & Ferrándiz, S. New Materials for 3D-Printing Based on Polycaprolactone with Gum Rosin and Beeswax as Additives. *Polymers* **12**, 334 (2020).
5. Verney, J. C. K. d., Lima, M. F. S. & Lenz, D. M. Properties of SBS and sisal fiber composites: ecological material for shoe manufacturing. *Mater. Res.* **11**, 447-451 (2008).
6. Liu, X. *et al.* An Electroactive Pure Organic Room-Temperature Phosphorescence Polymer Based on a Donor-Oxygen-Acceptor Geometry. *Angew. Chem. Int. Ed.* **60,** 2455-2463 (2021).
7. Fu, Y. *et al.* Boosting external quantum efficiency to 38.6% of sky-blue delayed fluorescence molecules by optimizing horizontal dipole orientation. *Sci. Adv.* **7**, eabj2504 (2021).